PNNL-11392
UC-713

Pacific Northwest
National Laboratory

Operated by Battelle for the
U.S. Department of Energy

Capillary Optics for Radiation Focusing

A. J. Peurrung
P. L. Reeder
M. Bliss
R. A. Craig
E. A. Lepel
D. C. Stromswold
J. Stoffels
D. S. Sunberg
H. Tenny

November 1996

Prepared for the U.S. Department of Energy
under Contract DE-AC06-76RLO 1830

PNNL-11392

DISCLAIMER

PACIFIC NORTHWEST NATIONAL LABORATORY
operated by
BATTELLE
for the
UNITED STATES DEPARTMENT OF ENERGY
under Contract DE-AC06-76RLO 1830

Printed in the United States of America

Available to DOE and DOE contractors from the Office of Scientific and Technical Information, P.O. Box 62, Oak Ridge, TN 37831; prices available from (615) 576-8401.

Available to the public from the National Technical Information Service, U.S. Department of Commerce, 5285 Port Royal Rd., Springfield, VA 22161

PNNL-11392
UC-713

Capillary Optics for Radiation Focusing

A. J. Peurrung
P. L. Reeder
M. Bliss
R. A. Craig
E. A. Lepel
D. C. Stromswold
J. Stoffels
D. S. Sunberg
H. Tenny

November 1996

Prepared for
the U.S. Department of Energy
under Contract DE-AC06-76RLO 1830

Pacific Northwest National Laboratory
Richland, Washington 99352

Summary

Capillary lens technology may ultimately bring benefits to neutron and x-ray-based science commensurate with the benefits provided by conventional lenses that focus visible light. A capillary lens consists of a large number of hollow capillaries, each of which gathers some fraction of the available incident radiation and guides it so that all of the transmitted radiation is directed for maximum utility. (Often, the outgoing radiation is made to converge at a common focal point.) Although the technology for capillary optics is not yet 10 years old, these lenses have already had a significant impact in a number of areas of engineering, science, and medicine. In general, capillary lenses provide maximum advantage whenever it is desirable to increase the radiation flux at a specific location without regard to its angular divergence. In the future, more efficient capillary lenses will probably be developed that achieve much higher intensity gains by guiding radiation to a smaller focal point. These anticipated improvements can only widen the range of applications for which capillary lenses are well suited.

Pacific Northwest National Laboratory (PNNL) has worked to improve this technology in a number of ways. A neutron-sensitive fiber optic faceplate may greatly shorten the time required for experimental measurements involving capillary neutron lenses. A single, optimally tapered capillary was manufactured at PNNL. This *single* taper allows intensity gains of a factor of 270 to be achieved for an initially parallel, incident x-ray beam. The feasibility of two separate methods that might be used to construct neutron lenses incorporating ^{58}Ni and thus having improved focusing power has been explored at PNNL. The isotope ^{58}Ni is particularly effective at reflecting neutrons, a critical factor in the construction of neutron lenses. First, it might be possible to use glass rich in this isotope. Second, it might be possible to construct capillary lenses constructed entirely from metal capillaries. These metal capillaries could then either be composed of or coated with nearly pure ^{58}Ni. Each of these improvements to capillary lens technology is discussed in Section 3.0.

In addition to striving for fundamental technological advances, PNNL has identified and investigated three applications for capillary optics. First, a capillary neutron lens should be capable of measuring the strength of a neutron-emitting source from substantially greater distances than allowed by conventional methods of neutron detection. The device that accomplishes this measurement has been dubbed the "neutron telescope." Second, a capillary x-ray lens has been acquired and studied for the application of small-particle diffractometry. Although current technology can identify small crystalline particles through diffractometry, measurement times can be as long as one week. It is hoped that ultimately x-ray lenses will shorten this time by 1-2 orders of magnitude. Finally, an investigation of the use of capillary lenses for neutron radiotherapy of deep-seated tumors was completed. It was found that significantly more cost effective therapy may be possible with the use of a capillary optic. Each of these applications is discussed in Section 4.0.

The final section of this report concludes by providing a brief guide to determining which potential applications are likely to be helped by capillary optics. In short, what capillary optics cannot do is just as important as what they can do. Capillary lenses do not operate on radiations other than thermal neutrons, sub-thermal neutrons, and x-rays with energies between roughly 1 and 10 keV. Capillary optics can bend radiation (this is how focusing is achieved), but not along a path with a radius of curvature greater than roughly 1 meter. No capillary optic has yet been constructed with a diameter greater than roughly 4 cm or a length greater than roughly 20 cm. Any capillary optic must obey the Liouville theorem; i.e., bringing the radiation to a narrow focus *must* necessarily increase its angular divergence. The final section of this report, Section 5.0, discusses these limitations and how they govern the selection of applications for which capillary optics are well suited.

Contents

Figures

Tables

1.0 Introduction

1.1 History

M. A. Kumakhov designed and constructed the first capillary lens at the I. V. Kurchatov Atomic Energy Institute in Moscow, Russia, in the late 1980s. Although this first generation lens was nothing like current lenses in terms of quality or capability, it was sufficient to demonstrate the practicality of soft x-ray focusing (Mosher and Stephanakis 1976; Kumakov and Komarov 1990; Mildner 1990a). Kumakhov brought his technology to the United States shortly thereafter, where he teamed up with Professor Walter Gibson in the physics department of the State University of New York at Albany. Soon Professor Gibson and his son, David Gibson, had formed a company, X-Ray Optical Systems, with the goal of commercializing this incipient technology. As of 1996, this company has sold roughly 10 lenses and holds a number of crucial patents related to capillary optics technology. In addition to intellectual property, this company has acquired invaluable expertise in the "art" of lens construction. Several "off-the-shelf" lens designs can be purchased for several tens of thousands of dollars. Although the ultimate future of this technology is not certain, X-Ray Optical Systems is sure to play a major role in any future lens development activity.

It did not take long for capillary optics to find application in the arena of neutron focusing. It is a fortunate circumstance of nature that the *very same* capillary lenses can be used to focus both x-rays and thermal neutrons (Chen et al. 1992; Mildner et al. 1993). Staff at the National Institute of Standards and Technology (NIST) have led efforts to demonstrate the utility of neutron focusing for numerous applications. They possess the world's best neutron lens, which has demonstrated a neutron fluence gain of a factor of 80.

This technology recently garnered an "R&D 100" award and appears poised to numerous application areas, including national security, medicine, and electronic circuit manufacturing. More than a dozen separate institutions have investigated lens behavior under a variety of applications. Indeed, the capillary lens can be considered a permanent member of the set of tools available to practitioners of the physical and biological sciences.

Pacific Northwest National Laboratory (PNNL)[(a)] has worked to improve this technology in a number of ways. For example, a single, optimally tapered capillary was manufactured. Also, the feasibility of two separate methods that might be used to construct neutron lenses incorporating ^{58}Ni has been explored. In addition to striving for fundamental technological advances, PNNL has identified and investigated three applications for capillary optics. 1) a "neutron telescope" to measure the strength of a neutron-emitting source from greater distances than is now possible, 2) a time saving capillary x-ray lens to apply to small-particle diffractometry, and 3) a capillary lenses for neutron radiotherapy of deep-seated tumors that could be less expensive than current therapies.

(a) Pacific Northwest National Laboratory is operated for the U.S. Department of Energy by Battelle under Contract DE-AC06-76RLO 1830.

1.2 Basic Principles of Capillary Lens Operation

Strictly speaking, the term capillary "lens" is a misnomer. A conventional optical lens relies on the *refraction* of light, i.e., the fact that a light quanta is bent, or redirected, when entering a material with a different index of refraction. In contrast, neutrons and x-rays are simply *reflected* from the inner surfaces of the hollow capillaries that make up the lens. In fact, a capillary lens has more in common with a fiber optic light guide or a garden hose than with a conventional optical lens. A schematic diagram of a neutron lens is shown in Figure 1.1.

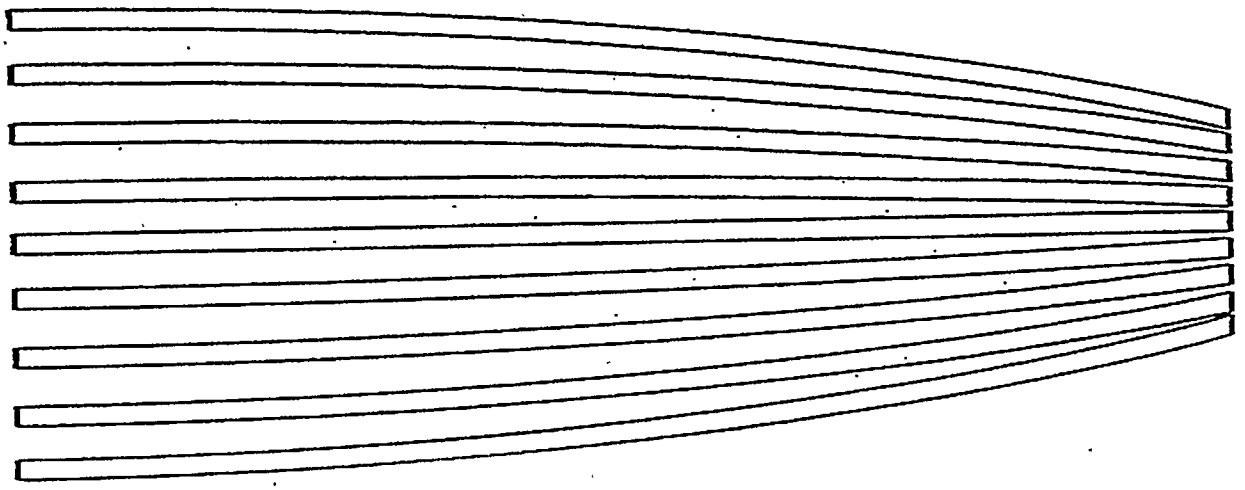

Figure 1.1. Schematic Side View of a Typical Capillary Lens

The lens is like a fiber optic light guide because both devices trap radiation through the process of total internal reflection. The lens is like a hose, however, because it is critically important that the radiation exiting the capillaries goes straight. Only in this way can the radiations from the various capillaries that make up a lens bring their component radiations to the same focal point.

An obvious question concerns the mechanism by which neutron or x-ray radiation is reflected from the inner walls of the lens' capillaries. The simple answer to this question is that common materials such as glass and metal have effective indices of refraction that are slightly *less* than one. Since the index of refraction of the air inside the hollow capillaries is almost exactly 1.0, radiation can be reflected at the inner capillary wall as the radiation first encounters material with a lower index of refraction. As is the case with conventional optics, the index of refraction for x-rays and neutrons depends on energy (wavelength). For this reason, sensible use of capillary optics is limited to neutrons with energies below roughly 0.05 eV and x-rays with energies below roughly 10 keV. In addition, x-rays below roughly 1 keV are hard to focus because absorption becomes a serious problem. Fortunately, these useful energy ranges include both thermal and sub-thermal neutrons as well as x-ray bands commonly used for medical, lithographic, and analytical applications. Generally speaking, a capillary neutron lens will have no effect on radiation of an energy that lies above the indicated ranges.

Capillary lenses can be used to accomplish several fundamentally different tasks. Perhaps the simplest class of lenses are called "benders." These lenses simply enable radiation to turn through some angle, but have no other effect. This function, however, can be critically important for some applications. For example, a neutron beam that has rounded a corner can be brought to a location that has no direct, "line-of-sight" connection with the reactor core that is the neutron source. Full barrel lenses gather diverging radiation and redirect it as converging radiation that arrives at a common focus. This general function is referred to as "source transfer." Lastly, half barrel lenses can either focus radiation that is initially parallel, or turn diverging radiation into beam-like radiation with little divergence. Every application for capillary lenses requires one of these three types of lens.

The last point to stress about capillary lenses is that they can only "compress" radiation spatially at the cost of increased divergence. In other words, radiation at the focus of a capillary lens may be more intense, but it must come from a wider variety of directions. The physical theorem that governs this behavior is known as Liouville's theorem. It is important to understand this principle when considering applications for capillary lenses.

1.3 Applications

What follows is a list applications that have been considered for capillary lenses. For each application, the importance of a capillary lens is briefly discussed. Note that some of these applications are speculative; that is, actual use of a capillary lens may not have been seriously attempted.

X-Ray lithography: If an x-ray capillary lens were used to collimate (make parallel or non-diverging) x-ray radiation for lithography, a significantly higher quality process might be possible.

Weapons Simulation: In this application, it is desirable to separate the measurement site from the simulation site to avoid damage from the "debris" produced by the weapons simulation.

Beam Bending: Neutron beams at research reactors are being considered for numerous practical applications such as tomography. The quality and usefulness of these beams may be enhanced by moving the beam to a location out of line with radiation (fast neutrons, gamma rays) that originates in the reactor core.

X-Ray Diffractometry: The intensity of x-ray radiation that can be effectively used for diffractometry may be greatly increased with the aid of a neutron lens. This, in turn, may shorten the time required to acquire diffractometry data.

X-Ray Scalpel: A capillary lens could produce an x-ray flux intense enough for medical use at some distance from the x-ray source.

X-Ray Filtering: Because the capillary x-ray lens only passes x-rays from within a certain energy range, the lens itself can act as an x-ray energy band-pass filter.

X-Ray Fluorescence: As with other x-ray analytical techniques, x-ray fluorescence analysis may be aided with the use of a capillary lens. This may allow a reduction of the particle size at which analysis is feasible.

Neutron Activation Analysis: The flux increase that is possible with the use of a capillary lens may greatly increase the utility of neutron activation analysis. The consequent reduction in required source strength may allow portable systems that use ^{252}Cf neutron sources to become practical.

Medical X-Ray Imaging: An x-ray lens on the film side of a medical x-ray such as a mammogram can prevent scattered x-rays from reaching the film. This, in turn, can improve the quality of the resulting image by reducing background and enhancing contrast.

Neutron Radiotherapy: A neutron lens can be used to create a relatively intense, narrow thermal neutron beam that can be aimed directly at the site of a cancerous tumor. This technique has been shown to reduce the radiation dose received by healthy parts of a patient and within the treatment room generally. The cost of radiotherapy treatments may also be greatly reduced as a result of more efficient use of neutron resources.

Remote Neutron Source Localization and Measurement: A neutron detector placed at the focus of a neutron lens could be exceptionally small and therefore have a very low background count rate. In this way, it should be possible to construct a neutron telescope that measures the strength of a neutron source from a considerable distance.

1.4 The Future

Capillary lens technology is still young and continues to improve. As capillary optics technology improves, more and more applications will become economically viable or physically practical. Likely improvements to expect in the next several years are listed below.

Increased Efficiency: Improved materials and better construction techniques should allow significant improvements in the efficiency of both neutron and capillary lenses. This means, in essence, that more of the neutrons or x-rays striking the front surface of a lens will likely be accepted, guided, and transmitted through the lens.

Improved Neutron Acceptance: A lens constructed with any of several isotopes such as ^{58}Ni will enable more effective neutron focusing. This is because materials incorporating ^{58}Ni have indices of refraction that differ more substantially from unity. A four-fold improvement in the neutron gathering power of lenses may be possible.

Smaller Focal Spot Size: Improvements in lens construction technology will almost surely lead to a reduction in focal spot size. Since the same amount of radiation reaches a smaller area, the overall intensity gain can be tremendous.

2.0 The Science of Capillary Optics

2.1 Reflection

The effective index of refraction of the capillary material is *very* close to unity. As a result, total internal reflection occurs only for those neutrons or x-rays that strike the lens moving in a direction that is nearly parallel with the axis of the capillary involved. This situation has several important ramifications. In order to have a chance of being successfully acted upon by a capillary lens, incident radiation must be aligned with the individual capillaries of the lens to within an angle of roughly 4×10^{-3} radians. This angle is called the "critical angle." Misalignment angles significantly greater than this usually result in failure to accept radiation for focusing. Such a neutron or x-ray will either be absorbed or pass straight through the lens as if it were not there.

Calculating the index of refraction and related critical angle requires some knowledge of a particular material's properties. For x-rays, a critical parameter is the plasma frequency (ω_p) given by MacDonald et al. (1993)

$$\omega_p = Nq^2/m\epsilon_o \tag{2.1}$$

where N is the electron density, ϵ_o is the permittivity of free space, and q and m are the electron's charge and mass. The index of refraction (n) for a particular material can be calculated from the relation,

$$n^2 = 1 - (\omega_p/\omega)^2 \tag{2.2}$$

where ω is the photon's frequency. Snell's law relates the critical angle (θ_c) for total internal reflection to the index of refraction as follows:

$$\theta_c = (2[n-1])^{1/2} \tag{2.3}$$

This angle represents the maximum angle with which an x-ray can strike the capillary wall and still be reflected. For neutrons, the index of refraction can be calculated from (Kumakov and Komarov 1990)

$$n^2 = 1 - \lambda^2 Nb/\pi \tag{2.4}$$

where λ is the neutron De Broglie wavelength, b is the coherent scattering amplitude for the material, and N is the atom density. Using Snell's law again yields an expression for the critical angle for neutron reflection,

$$\theta_c = \lambda(Nb/\pi)^{1/2} \tag{2.5}$$

The need for effective radiation transmission through very narrow capillaries imposes strict requirements on the efficiency of total internal reflection within the capillaries (Mildner 1990b). A neutron or x-ray may undergo as many as 100 internal reflections during the transit of a 10-cm-long capillary. If the probability of absorption or diffuse scattering at each reflection is α, then the probability of successful transmission through the entire capillary is $(1-\alpha)^N$, where N is the total number of internal reflections. In practice, serious degradation of lens performance results whenever $\alpha > 0.01$. Satisfying this condition requires

capillaries with extremely smooth inner surfaces and minimal absorption to minimize neutron capture (Kimball and Bittel 1993; Pantell and Chung 1979).

2.2 Acceptable Radiation

Note that for both neutrons and x-rays, the critical angle is a decreasing function of energy. Any energy dependence of the index of refraction indicates a material that is dispersive. (Glass is slightly dispersive when transmitting visible light. This is why white light produces a rainbow when traveling through a glass prism.) Equations (2.1) through (2.5) demonstrate that glass is highly dispersive for both neutron and x-ray radiation. Thus, lenses can focus soft x-rays and thermal neutrons, but not hard x-rays, gamma-rays, epithermal neutrons, or fast neutrons. In fact, neutron lenses work most effectively for neutrons with energies even lower than thermal energies. Fortunately, many of the applications for neutron lenses rely on neutron beams from research reactors. Reactors with cold neutron sources can provide beams with energies that correspond to temperatures that are between 20K and 80K. Thermal neutrons can be focused, but the critical angle is roughly 2×10^{-4} radians at that energy (0.025 eV). The utility of x-ray focusing begins to seriously suffer above an energy of 10 keV.

The failure of x-ray lenses to transmit photons with energies below approximately 1 keV is not the result of the lens's optical properties. Instead, the capillaries themselves begin to strongly absorb photons below this energy. At first glance, this appears counter-intuitive. If a photon is reflected at the boundary between air and glass, how can the glass absorb photons? During the process of reflection, the photon actually penetrates a small but nonzero distance within the glass outer wall of the capillary. Absorption is possible because of this penetration. For a similar reason, it is advisable to use boron-free glass when constructing a lens designed to focus neutrons.

2.3 Bending

Constructing a useful capillary lens necessarily requires that individual capillaries guide radiation through a gradual curve. This process is illustrated in Figure 2.1. An approximate criterion for successful radiation transfer through a curve can be derived as follows. Assume that a particle (neutron or photon) travels within a straight capillary in such a way that it is reflected from the sides of the capillary at the critical angle, θ_c. If this particle "bounces" across the diameter of the capillary, then the particle travels a distance $2D/\theta_c$ during one cycle of this motion, where D is the capillary diameter. (Note that an infinity of alternate motions is possible.) Successful radiation transmission is likely whenever the capillary curves through an angle less than θ_c during each cycle of this motion. This informal criterion can be written as

$$\rho > 2D/\theta_c^2 \tag{2.6}$$

where ρ is the capillary's radius of curvature (Marten 1966; Kumakov and Komarov 1990). While the derivation of this criterion is clearly approximate, more careful investigations have basically confirmed its validity (Mildner 1990a; Mildner 1990b) The implications of Eq. (2.6) are profound. Since the critical angle has a value that is generally not greater than 4×10^{-3}, and a useful lens will require capillaries with a radius of curvature less than roughly 1 meter, Eq. (2.6) requires that the capillary diameter be less than 8 microns! Indeed, this is roughly the diameter currently used in constructing capillary lenses. A lens with a total cross-sectional area of 1 cm^2 therefore requires more than 10^6 individual capillaries. This is achieved by

constructing a lens from roughly 10^3 "polycapillaries," which in turn contain a large number of capillaries (Pantojas et al. 1993). The polycapillaries must be carefully bent and aligned during lens assembly to achieve the desired optical effect.

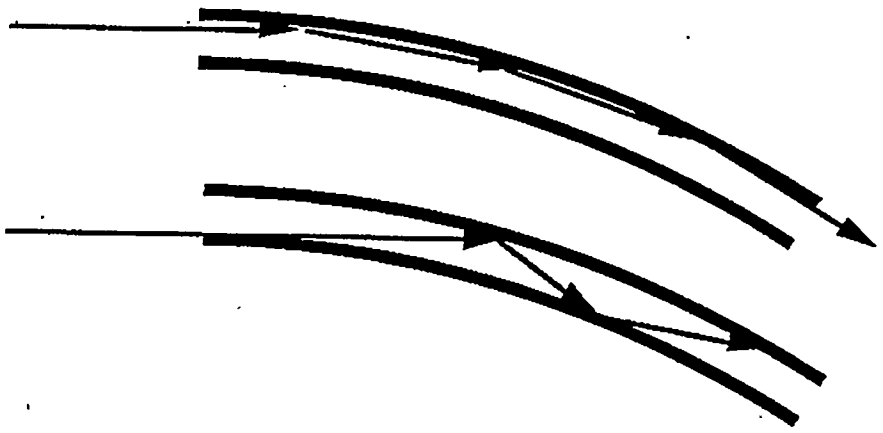

Figure 2.1 Guiding Radiation Through a Bent Capillary

2.4 Types of Lenses

Three basic types of capillary lenses are commonly constructed. Understanding the functions of these lenses requires a careful understanding of how lenses in general operate. The small value of the critical angle for reflection in these devices has important implications. First, only radiation that reaches a capillary at the front of a lens and is well aligned with that capillary can be accepted by the lens. Second, any radiation emerging from the back of the capillary lens will have a direction aligned with that of the guiding capillary to within the critical angle.

The three different types of capillary lenses use the above properties of capillary lenses in different ways. The lens drawn in Figure 2.1 is a "half barrel" lens. This type of lens has capillaries that are parallel at one end and converging at the other. The capillaries at the converging end of a well-constructed half barrel lens will all point to precisely the same point in space as shown in Figure 2.2.

However, no lens is perfect; the capillaries will on average be misaligned with each other by an angle $(\theta_m + \theta_c)$, where θ_m is the typical misalignment angle between capillaries. Assuming that the distance from the back of the lens to the focus is L_f, the focal spot will have a diameter at least as large as $(2\ [\theta_m + \theta_c]\ L_f)$. (The focal spot size is also affected by factors such as the critical angle and the size of the polycapillary bundles.) A half barrel lens in this configuration gathers initially parallel radiation and brings it to a common focus. Such a lens would be used for any application where it is desirable to intensify radiation from an initially beam-like source. Synchrotrons can produce parallel radiation beams, or they can be produced at large distances from any strong source, such as a nuclear reactor. A half barrel lens can also be turned around 180 degrees and used to collimate radiation that is initially diverging. Many radiation sources produce radiation that diverges from an effectively point-like source. However, some applications, such as x-ray

lithography or medical imaging, are optimized with well-collimated radiation. A half-barrel lens is ideal for such applications.

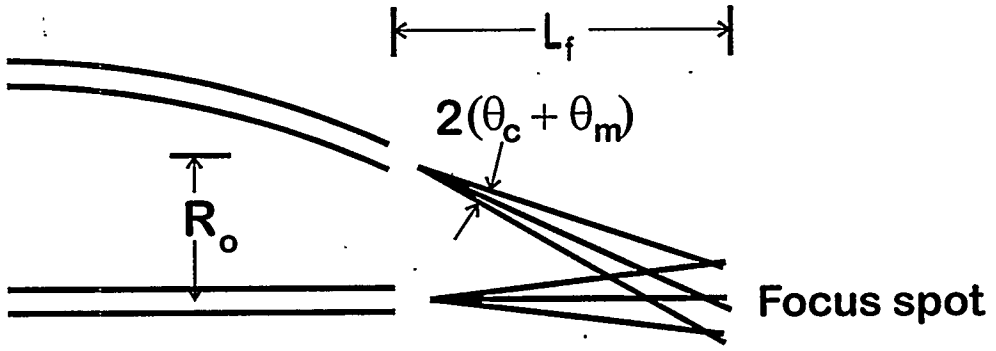

Figure 2.2. Diagram Using Ray Optics to Illustrate Focusing by a Half Barrel Lens

The second major type of lens is a full-barrel lens. A full-barrel lens could be constructed from two half-barrel lenses placed back to back in such a way that initially diverging radiation is brought to a focus. (In reality this method of construction is unlikely.) Figure 2.3 contains a sketch of a full-barrel lens. Full-barrel lenses are used for applications where a "source transfer" is desired, i.e., where it is desirable to recreate much of the radiation intensity associated with a particular source without the hazards or disadvantages associated with intimate physical proximity with the source. Two different applications for a full-barrel lens are detailed later in this report.

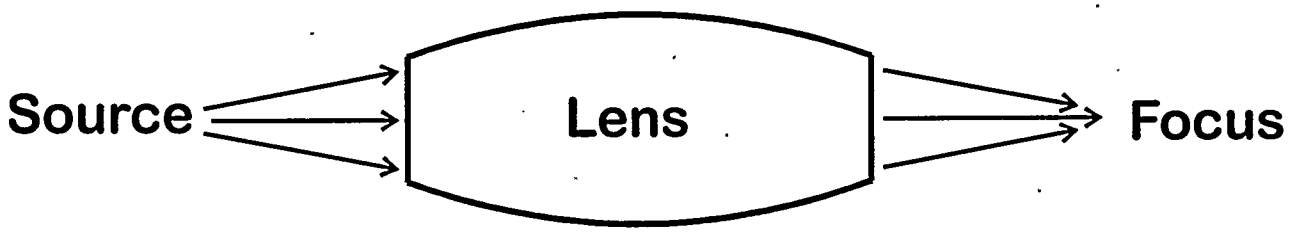

Figure 2.3. Sketch of a Full-Barrel Lens

The final and possibly simplest type of lens is a bender. These lenses simply enable radiation to turn through some angle, but have no other effect. This function, however, can be critically important for some applications. For example, a neutron beam that has rounded a corner can be brought to a location that has no direct, "line-of-sight" connection with the reactor core that is the neutron source.

2.5 Liouville's Theorem

One fundamental physical constraint affects the performance of all capillary lenses. The Liouville's theorem says that the *phase space* volume occupied by radiation can not be altered by the action of a capillary lens (or any other system.) Assuming that the radiation takes the form of a cylindrical beam with spatial radius R and angular divergence θ, Liouville's theorem requires that the product $R\theta$ be the same before and after radiation passes through a capillary lens. In other words, it is possible to "compress" a radiation beam with a capillary lens, but only at the cost of increased angular divergence. Such an increase in divergence does not matter for many applications for which the radiation direction is irrelevant, such as neutron activation analysis, x-ray fluorescence, etc. However, this constraint has important implications for some of the applications for which a capillary lens might be considered. A typical example of such an application is x-ray diffractometry, for which it is desirable to have the maximum radiation intensity *and* the minimum radiation divergence. Increased intensity allows diffractometry data to be acquired in less time, but increased divergence worsens resolution and may hinder the identification of features in the data when background is present. In summary, it is critical to consider for a particular application whether intensifying the radiation is all that is desired, or whether it is necessary to increase the radiation intensity without a concomitant increase in the divergence.

2.6 Efficiency and Gain

The efficiency of a capillary lens must be carefully defined and even more carefully estimated. We here define efficiency to be the quantity of incident radiation that is accepted, guided, and transmitted by the lens divided by the quantity of incident radiation that could ever possibly be accepted, guided, and transmitted. Remember that in order for radiation to have a chance of being accepted by the lens, it must strike the lens traveling at an angle less than the critical angle relative to the axis of the nearest capillary. The efficiency quantifies the degree to which a particular lens approaches the ideal possible performance. Efficiency does not, for example, depend directly on the critical angle, even though the critical angle clearly affects the behavior of any particular lens.

The gain of a capillary lens specifically quantifies the intensification of radiation that a lens makes possible. Suppose that a particular lens has an efficiency E, gathers all of the radiation from a circular area with radius R_1, and focuses this radiation down to a focal spot with radius R_f. The gain of this lens would be

$$G = CE(R_1/R_f)^2 \tag{2.7}$$

where C is the capture fraction, or fraction of the incident radiation that strikes the lens at less than the critical angle. A higher critical angle can lead to a higher lens gain through one of the following mechanisms. First, it may allow the lens to capture a larger fraction of the incident radiation; i.e., C may increase. Second, a larger critical angle allows more severe capillary bending according to Eq. (2.6). Thus a lens with a higher critical angle can be redesigned to have a smaller focal length and smaller focal size, R_f.

A capillary lens for a typical application may have an overall efficiency E=10%, and a gain of roughly G=100. The capture fraction depends simply on the properties of the incoming radiation through the relation

$$C = (\theta_c/\theta_d)^2 \qquad (2.8)$$

where θ_d is the divergence angle for the incident radiation. A complete discussion of what determines the efficiency of a lens is given in Section 3.5. The discussion is included there as one of the areas where PNNL has made a significant contribution to capillary lens science.

3.0 PNNL's Advances

This section describes a number of separate areas where PNNL has contributed to the science or technology of capillary lenses generally. Other than this, the six subsections below are not connected. The following list contains a brief synopsis of each of these technical areas.

- PNNL has constructed a neutron-sensitive fiber optic faceplate that may prove useful as a thermal neutron beam diagnostic. This device may ultimately speed the collection of data with capillary neutron lenses.
- PNNL has supported the development of single tapered capillaries. Capillaries of this sort will likely find use for lens construction in the future. Far higher intensity gains are possible.
- PNNL has investigated the feasibility of using nickel-loaded glass to construct a neutron lens with a larger critical angle. Such a lens would have the advantages of glass, but improved neutron focusing power.
- PNNL has reviewed the extensive literature concerning the reflection of radiation from rough surfaces and arrived and several conclusions of relevance to capillary optics.
- PNNL has experimentally studied the reflectivity of metal capillaries. If such capillaries were sufficiently reflective, a significantly more powerful neutron lens could be constructed. It was found that metal surfaces are too rough to reflect sufficiently well. In addition, these surfaces are not helped by surface treatments such as electropolishing and chemical polishing.
- PNNL has carefully analyzed the efficiency of neutron lenses. Our treatment of this subject is useful when new applications for capillary lenses are considered.

3.1 Diagnostic Faceplate

A common problem in the use of capillary neutron lenses is determining the location and spot size of beams of slow neutrons (cold, thermal, or epithermal). A related need is in neutron radiography where a real-time, electronic detection system would be a major improvement over the radiographic film techniques presently in use. In this case, low cost, large area detectors up to 1 m^2 are desired. Although it would be highly intrusive, a neutron imaging system could be used to inspect nuclear weapon assemblies. A neutron imaging system might be combined with a collimating array to provide enhanced capabilities.

A neutron imaging system is currently being used by the Nuclear Methods Group on neutron beams at the NIST reactor. The detector consists of a charge induction device (CID) semiconductor camera covered by a thin film of ^{6}LiF. The recoil charged particles (tritons and alphas) from neutron capture on ^{6}Li impinge on the face of the CID semiconductor and give an electronic pulse typically within a single pixel. The pixel size of the CID is 0.011 by 0.011 mm^2, so this device provides excellent position resolution. However, the ^{6}LiF coating must be thin to allow the recoil particles to escape into the CID. Thus, the neutron capture efficiency is only about 2%. The detector area is limited to the size of the CID device, which is about 1 cm^2.

We have developed a preliminary neutron imaging system based on a scintillating fiber faceplate. The faceplate captures the thermal neutrons in ^{6}Li silicate glass fibers and produces a pulse of light that is detected by an appropriate photodetector. The scintillating fibers are arranged perpendicularly to the face of the position-sensitive photodetector. The light is channeled to travel within a single fiber so the position

resolution is governed by the diameter of the scintillating fibers. The neutron sensitive scintillating fibers made by PNNL typically have diameters of 0.12 mm, but fibers could be produced with diameters a factor of 2 higher or lower. The scintillating fiber faceplate does not give the high position resolution characteristic of the CID device. However, the 0.12-mm pixel size is adequate for many applications. A major advantage of the fiber faceplate is that the density of ^{6}Li in the glass is sufficient to capture almost all the neutrons in a length of about 2 mm. The scintillating fiber faceplate could be used with a variety of position-sensitive photodetectors, including position-sensitive photomultiplier tubes, the CID camera, or the recently developed large-area, amorphous silicon diode arrays with areas up to 40 by 40 cm^2. Thus, the scintillating fiber faceplate should have good position resolution, >80% efficiency for neutron capture, and the capability for low-cost, large-area detectors.

Faceplates made from PNNL scintillating glass fibers have been produced in thicknesses ranging from 1.32 to 3.2 mm. The pulse-height spectra for these faceplates were measured by mounting them on a standard photomultiplier tube and irradiating them with thermal neutrons. The spectra for three different thicknesses are shown in Figure 3.1. The amplitude of the thermal neutron peak is inversely related to the thickness due to attenuation of the scintillation light within the glass fibers. The centroid of the neutron peak is plotted in Figure 3.2 as a function of the faceplate thickness. The light output of these peaks corresponds to between 200 to 300 photoelectrons, which is enough light to consider using them with position sensitive photodetectors.

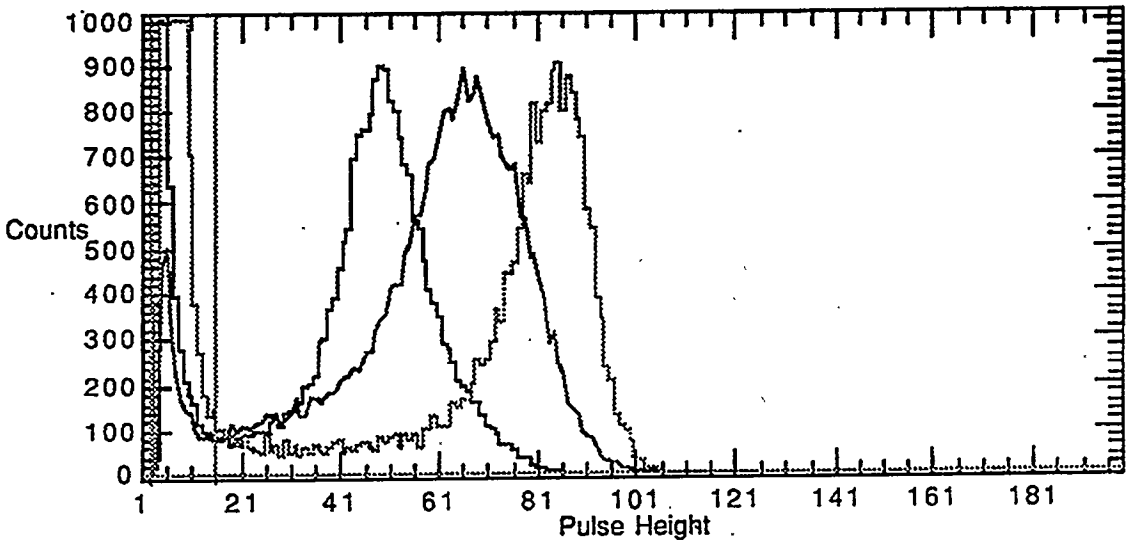

Figure 3.1. Pulse-Height Spectra for Thermal Neutron Capture in Scintillating Fiber Faceplates of Three Different Thicknesses. Faceplate thicknesses were 3.20 mm, 1.59 mm, and 1.32 mm in order of increasing light output.

Fiber faceplates were manufactured by packing fibers into shrink tubing and then forcing a casting resin into any open channels to form a rigid cylinder. The cylinder was then sliced into thin wafers of the desired thickness. Both sides of the wafer were then polished. One faceplate was made with a modified technique that gave a more compact bundle that was easier to polish. Scintillating glass fibers containing enriched ^{6}Li were laid horizontally in a semicircular trough having a 12.7-mm radius and bonded with the epoxy compound "Epo-Thin." A vacuum was pulled to remove any air bubbles. Two thin slices were cut perpendicular to the axis of the trough and polished to a thickness of about 1.6 mm. The two semicircular pieces were mounted together to form a circular faceplate with a diameter of 25.4 mm. The joint between the two halves was estimated to be about 1.3 mm. This faceplate was mounted on a position-sensitive photomultiplier tube and exposed to a flux of thermal neutrons. The resulting image shown in Figure 3.3 clearly shows the circular image of the faceplate and the dividing line between the two halves. The data were obtained in an array of 100 by 100 channels, which limited the pixel resolution to 1 channel by 1 channel. The image had a total width of about 40 channels, which corresponds to an actual distance of 25.4 mm. Thus the pixel resolution is about 0.63 mm by 0.63 mm. This pixel size is much greater than the diameter of the individual fibers (0.12 mm), so individual fibers are not resolved in this image. The full-width half maximum (FWHM) of the measured valley was about 3.5 channels or 2.2 mm, which is reasonably consistent with the estimated separation of 1.3 mm.

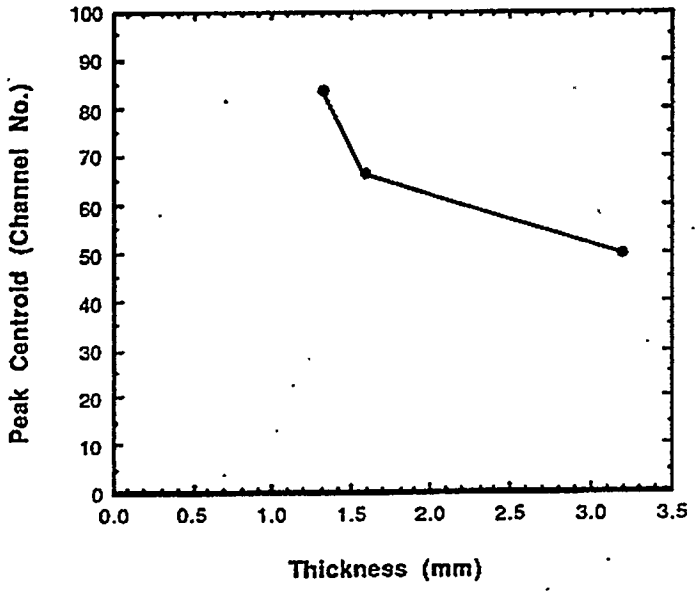

Figure 3.2. Relative Light Output from Three Different Thicknesses of Scintillating Fiber Faceplates

This test demonstrated the possibilities of the scintillating fiber faceplate for use in imaging neutron beams. Much improvement in resolution can be expected in going to a thinner faceplate and smaller diameter fibers. The thinner faceplate gives higher light output per event and improves the calculation of the position of that event. Smaller diameter fibers will give enhanced position resolution because the size of the light spot from a given event is governed by the diameter of the fiber in which the event occurred.

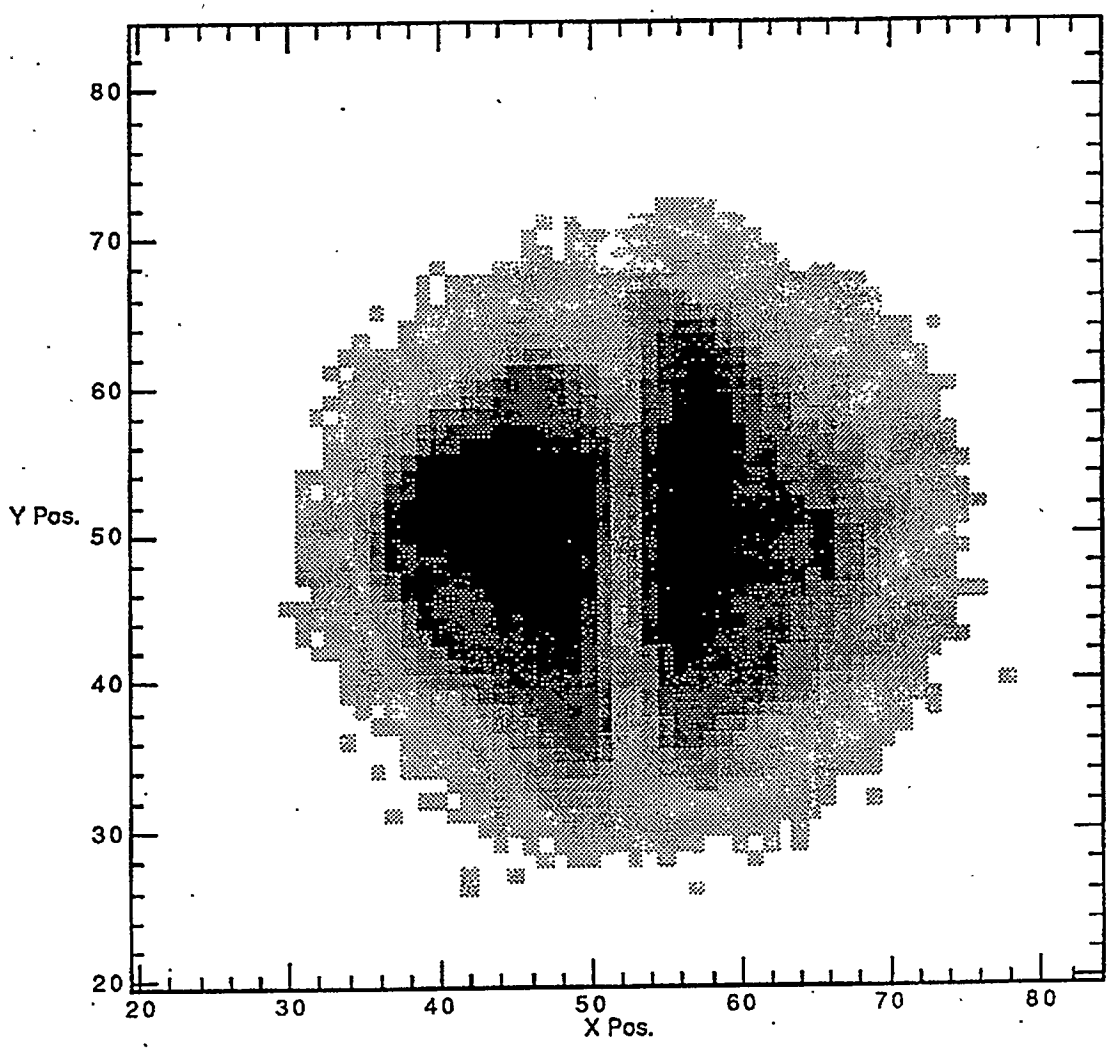

Figure 3.3. Image Produced by Neutron Irradiation of Faceplate Made with Two Semicircles

Another circular faceplate was prepared that was 11.1 mm in diameter and 1.3 mm thick. The image produced by this faceplate when mounted on the position-sensitive phototube is shown in Figure 3.4. The 11.1-mm faceplate appears to have a width of 20 channels corresponding to a pixel resolution of 0.55 mm by 0.55 mm. The disk was irradiated uniformly with neutrons, so the nonuniform response is due to imperfections in the faceplate. This faceplate was mounted in an adapter, which allowed it to be attached to the CID camera at NIST. Our goal was to determine whether enough photons are produced in the scintillating fibers to give signals above the noise threshold of the CCD camera.

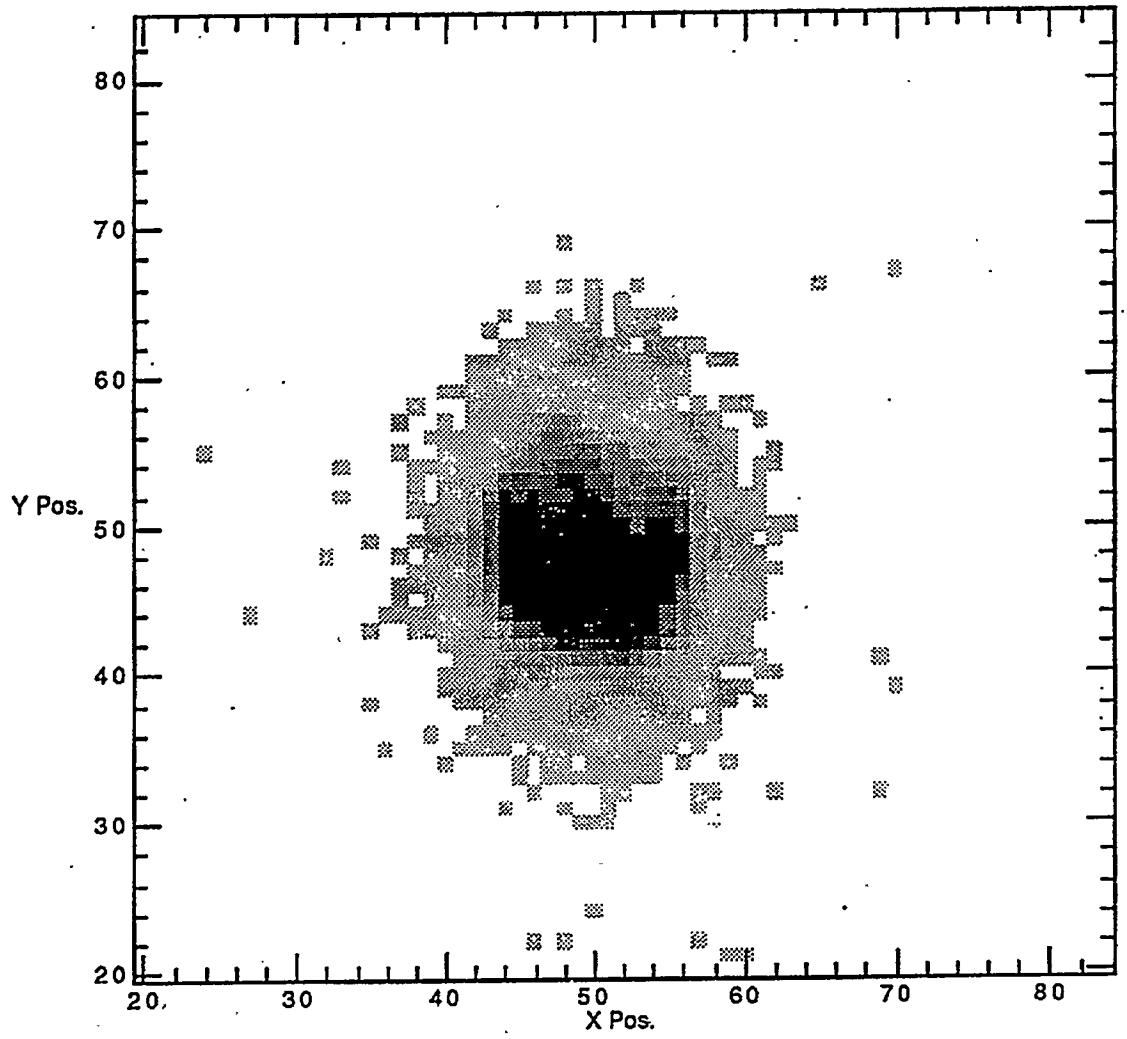

Figure 3.4. Position-Sensitive Photomultiplier Image from Neutron Irradiation of the Faceplate Mounted for Use with the CID Camera

The scintillating fiber faceplate was tested at a cold neutron beam line at the NIST reactor. The faceplate was attached to a CID camera that had no ^{6}LiF covering. The neutron beam was collimated to a 0.5-mm-diameter circle. As the pixel size of the CID camera (0.011 mm) was much smaller than the fiber diameter (0.12 mm), we expected that the camera might be able to resolve individual fibers in the faceplate. The light output of the faceplate was only slightly above the noise level of the CID camera, but by raising the electronic threshold of the CID camera, we were able to obtain the image shown in Figure 3.5. The image shows bright spots corresponding to enhanced light output from individual fibers and an overall circular shape corresponding to the 0.5-mm-diameter neutron beam. It is possible that the events that exceeded the electronic threshold are due only to events where two or more neutrons gave a simultaneous light pulse. It is also clear that the response of individual fibers was nonuniform. Improvements in the fiber faceplates are needed; however, this first result demonstrates that the use of scintillating fiber faceplates is feasible for imaging neutron beams.

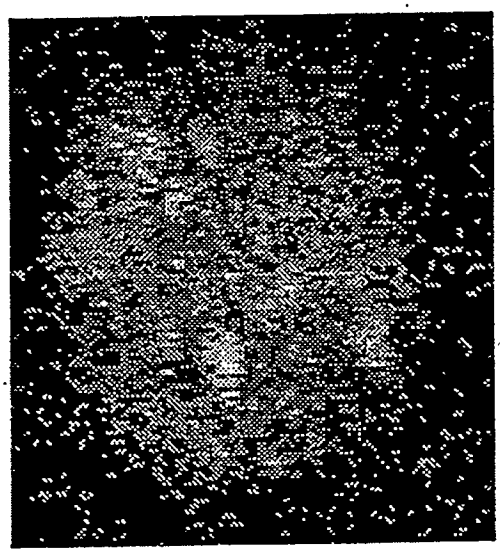

Figure 3.5. Image Obtained with Scintillating Fiber Faceplate Mounted on CID Camera at NIST

3.2 Tapered Capillaries

One of the current limitations of capillary optical technology is that the focus spot size can be no smaller than roughly 0.5 mm because of the finite size of polycapillaries, polycapillary misalignment, and the non-zero critical angle. This limitation can be overcome under some circumstances using a single hollow glass capillary that is specially tapered (Thiel et al. 1989; Hoffman et al. 1994) Figure 3.6 shows the focusing action that occurs inside a tapered capillary. This technique requires an extraordinarily parallel incident radiation beam and is therefore of primary interest for synchrotron-produced x-ray beams. However, under these conditions, the focus spot size is limited only by one's ability to draw hollow glass tubes down to sufficiently small sizes. The capillary project has partially sponsored an effort in the PNNL glass shop to produce tapered capillaries for this purpose. Eventually, this technology promises to allow x-ray analysis of materials with a spatial resolution far smaller than what is possible today.

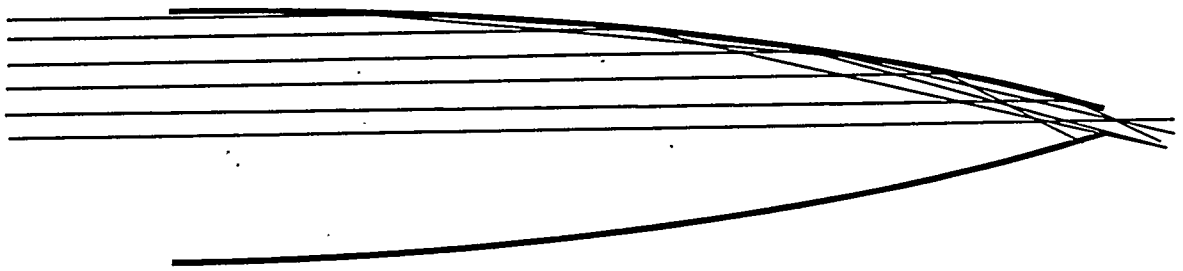

Figure 3.6. Focusing Action Within a Single, Tapered Capillary

3.3 Nickel-Loaded Glass

The usefulness of any capillary for polycapillary lens construction depends on smoothness and critical angle. Smooth surfaces are necessary to maximize reflection. Only glass capillaries have been shown to be sufficiently smooth for use in capillary lenses (see Section 3.4.) Metal surfaces, especially those using ^{58}Ni, provide the highest critical angle and therefore the highest neutron focusing power. We have investigated the possibility of using nickel-loaded glass to provide both advantages in the same device.

Glasses offer the smoothest fabricated surfaces possible because, barring corrosion, they are controlled entirely by surface tension. Because glasses lack long-range order, no "lower energy surfaces" are available as in crystalline structures that influence surface topology. No crystal faces, domains, or grain boundaries are generated to minimize energy upon cooling.

To date, the state of the art in capillary waveguide production is dominated by silicate glasses, primarily lead glasses and borosilicate glasses. These general compositions have several characteristics in common. First, they are very stable as glasses over a broad temperature range, and second, they are easy to manipulate as viscous fluids. These glasses are optimized for fabrication and not for optical properties in the x-ray or neutron regime. Silicate glasses, generally, are made up of materials with small scattering lengths and, therefore, small critical angles. The critical angle in large neutron guides is enhanced by coating the glass with isotopically enriched nickel or with so-called "supermirrors" (the neutron equivalent of dielectric mirrors) composed of layers of titanium and iron.

It is desirable to increase the average scattering length of the components of the glass. Glasses from other composition families may have superior optical properties in the x-ray or neutron regime; however, they are not readily available commercially. Some of these are: germanate glasses, chalcogenide glasses, and metallic glasses. Germanate glasses are analogues of silicate glasses in which the silicon has been replaced by germanium. Germinate glasses behave similarly to silicate glasses, but they are more easily reduced to the metal. Germanate glasses often contain some silica and some can be obtained commercially. Chalcogenide glasses are based on Group VI elements (S, Se, Te) combined with Group IV elements (Si, Ge) and Group V elements (P, Si, Sb, Bi). The primary advantage of chalcogenide glasses is that they do not contain oxygen, which has poor optical properties at the wavelengths of interest. Chalcogenide glasses are just now becoming common commercially and are available in fiber form. They are sensitive to oxygen at high temperatures and

must be produced in closed atmospheres. Metallic glasses are generally rich in Ni, Fe, P, and Lanthinides and are also anoxic.

Metallic glasses require rapid quench rates because they have low melt viscosities. The most common production methods produce fine powders. Some compositions can be drawn into wire. Metallic-glass wire is commercially available (Metglas®, a Fe-Ni-Cr-P-B alloy) in diameters of ~200 μm. Conversion to capillary production requires that wire-drawing equipment be modified to inject air in the center of the wire to form the bore. This will increase the cooling rate of the material and so should not interfere with glass formation. Most metallic glass compositions (Table 3.1) are complex mixtures. This is consistent with the need to avoid the onset of crystallization during glass production. (Simple compositions have a low entropy of mixing and require shorter diffusion lengths for crystal growth, which will proceed exothermically once initiated.) Many of the good metallic-glass forming composition families are well suited for x-ray or neutron scattering.

Table 3.1. Metallic Glass Composition Families That Form Readily on Cooling From the Melt

Group	Representative Systems	Typical Composition Atom %
Major Systems		
T^2 (or noble) metal + Metalloid (X)	Pd-Si, Co-P, Fe-P-C, Ni-P-B	15-25 X
T^1 metal + T^2 metal (or Cu)	Zr-Cu,	30-65 Cu
	Y-Cu, Ti-Ni	30-40 T^2, Cu
	Nb-Ni, Ta-Ni	40-65 Ni
Miscellaneous Systems		
A metal + B metal	Mg-Zn	25-35 Zn
T^1 metal + A metal	(Ti-Zr)-Be	20-60 Be
Actinide + T^1 metal	U-V, U-Cr	20-40 T^1
Where: T^1 = early transition metal (Sc, Ti, V groups), T^2 = late transition metal (Mn, Fe, Co, Ni groups), A metal = alkali and alkaline earths (Li, Mg groups), B metal = Cu, Zn, Al groups, Metalloid = B, C, Si, Ge, P.		

Some properties of glasses with characteristics relevant to neutron guiding are listed in Table 3.2. The densities used are based on published values for the crystalline material. Because metallic glasses have a wide composition range, the calculated properties of the metallic glass were based on a simple binary alloy. The thermal neutron capture cross-section is listed as well. This parameter is relevant because, during the reflection, the neutron wavefunction is sampling the guiding material and thus can react. The critical solid angle, as quoted in Table 3.1, is the solid angle subtended by the critical angle and is a measure of numerical aperture; the following column is the ratio of the solid angle to that for silicate glasses. The scattering length and capture cross-section are listed in Table 3.3 for isotopes that might be alloyed into metallic glasses to modify the scattering length.

Table 3.2. Properties of Some Glasses for Use in Neutron Guiding

Glass	Specific gravity	Molecular weight	Average scattering length (fermi)	1-Refractive index	Critical angle (milli-radian)	Critical solid angle/4 pi	Critical solid angle relative to SiO_2	Molecular average capture cross-section (barns)
SiO_2	2.65	60	5.3	7.20E-07	1.20	3.60E-07	1	3.5
GeO_2	6.239	105	7.3	1.34E-06	1.64	6.70E-07	1.86	7
$GeSe_2$	5.6	152	11.4	1.30E-06	1.61	6.48E-07	1.80	16.7
Metallic glass ($Ni_{0.8}P_{0.2}$)	7.255	53	12.5	5.25E-06	3.24	2.63E-06	7.30	21.5

Table 3.3. Scattering Length and Reaction Cross-Sections for Some Isotopes Relevant to Neutron Guiding Glasses

Isotope	Scattering Length (Fermi)	Capture Cross Section (barns)
^{58}Fe	15	28
^{164}Dy	49.4	307
^{196}Hg	30.3	115
^{58}Ni	14.4	26

Conclusions: Although the scattering lengths of germanium and selenium isotopes are greater than those for silicon and oxygen, replacing them gives a reduced effect because of the associated volume increase. In the case of metallic glasses (assumed to have the atomic volumes of the elements), the potential increase in numerical aperture is nearly an order of magnitude. Further optimization by adding stabilizing lanthanide atoms could be investigated.

This discussion has centered on guiding neutrons. Alternative materials may also improve guiding of x-rays as well, depending on the energy of the x-rays to be guided. The constituents of silicate glasses are largely light elements; these elements have resonances in the soft x-ray region. These resonances act both to affect the refractive index and the extinction coefficient of the guiding material. In those cases for which the important x-ray wavelengths are negatively affected by resonance absorptions, alternative glasses can be considered.

3.4 Surface Roughness

This section applies existing results in the field of small-angle scattering from rough surfaces to the problem of capillary optics. This subject has a long history and an extensive body of literature, both of which result from the inherently complicated nature of this problem. No one treatment of surface scattering is valid under all conditions; exact results are possible only via numerical computation. An additional complication arises from the general lack of detailed knowledge of the character of real surfaces at the 10^{-10} to 10^{-5} meter length scales. Fortunately, recent work has focused on the application of existing results to the specific problem of x-ray capillary optics (Chapman et al. 1993; Kimball and Bittel 1993).

The main points contained within this section are summarized as follows:

- The passage of x-rays through glass capillaries and neutrons through metal capillaries are optically analogous processes. The effect of surface roughness in the two cases should be similar.
- The 6Å figure often mentioned for the critical surface roughness is not without merit. However, this figure comes with several caveats and should not be discussed in isolation.
- The relationship between capillary optical performance and material index of refraction is not completely straightforward. In other words, both pros and cons are associated with a material like ^{58}Ni.

3.4.1 Preliminary Definitions

Let the function z(x,y) represent the height profile of an actual surface, and let

$$\sigma = (\langle z \rangle)^{1/2} \tag{3.1}$$

be the root of the mean square (RMS) height variation with $\langle z \rangle = 0$ assumed. The correlation function

$$C = \langle z(r)z(r+\rho) \rangle / \sigma^2 \tag{3.2}$$

describes the random variations in the surface height. The nature of these variations is generally parametrized by σ and τ, where τ is the "correlation" length that satisfies

$$C(\tau) = C(0)/e \tag{3.3}$$

Note that representing an entire surface roughness by two scalar numbers is a significant simplification, but one that is unavoidable considering the limited knowledge of surface characteristics and the need for simplicity.

Two additional parameters of interest for problems of small-angle, rough-surface scattering are the "path length" P and the "penetration depth" D. The penetration depth is actually the decay length of the evanescent wave that propagates into the surface when the scattering angle is less than the critical angle θ_c. This distance is best thought of as the "glancing angle skin depth." A calculation of D begins with Snell's law,

$$n_i \cos(\theta_i) = n_t \cos(\theta_t) \tag{3.4}$$

where n_i and n_t are the indices of refraction for the incident and transmitting materials, respectively. Note that the angles here are defined as the complements of the angles usually used in Snell's law. Substituting $n_i = 1, \theta_i = 0$, and $n_t = (1-\delta)^{1/2}$, we arrive at

$$\theta_i = (-\delta)^{1/2} \tag{3.5}$$

which clearly shows that the transmitted wave is evanescent. For an incident wave with wavevector k_i, it can be easily shown that the wavevector normal to the surface of the transmitted wave is $k_t^{\perp} \sim k_i \theta_t$, allowing us to write the penetration depth as

$$D = 1/k_t^{\perp} = 1/k_i \delta \tag{3.6}$$

For an electromagnetic wave of frequency ω, $\delta = \omega_p^2/\omega^2$, and this equation yields $D \sim c/\omega_p$ where c is the speed of light and ω_p is the "plasma" frequency in the transmitted material. For most glasses, $D \sim 60$Å. For neutrons with a de Broglie wavelength λ, $\delta = Nb\lambda^2/\pi$ where N is the material's atom density, and b is the coherent scattering length for neutrons. It follows that for neutrons, $D \sim (4\pi\, Nb)^{-1/2}$ or $D \sim 53$ Å for ^{58}Ni. The path length is the total distance traveled "underneath" the surface by an x-ray (or neutron) incident at the critical angle θ_c. The path length can therefore be written

$$P = 2D/\theta_c \tag{3.7}$$

3.4.2 Results

A more complete presentation of this topic is contained in the work by Kimball and Bittel (Kimball and Bittel 1993). For more information, this work should be consulted directly. The primary assumption needed for these results is that $(\sigma/D)^2 << 1$. Note that surface height variations with long correlation length τ would almost certainly violate this assumption. In other words, these results do not apply to surfaces with large-amplitude, long-wavelength roughness.

The effect of surface roughness is contained in the parameter ΔR, which denotes the decrease in the specular reflection coefficient. Only the specularly reflected component has a high probability of complete transmission through a capillary element. The loss ΔR depends in general on the three dimensionless parameters Λ, ν, and ϕ: Λ is the scaled RMS surface height σ/D, ν is the incident angle scaled to the critical angle θ_i/θ_c, and ϕ is the scaled correlation length τ/P. The effect of roughness on reflection is most severe when $\phi \sim 1$. Under this condition, the decrease in the specular reflection coefficient is given by

$$\Delta R \sim \nu \Lambda^2 \tag{3.8}$$

This result must be multiplied by $(8\phi)^{1/2}$ when $\phi << 1$ and $1/\phi$ when $\phi >> 1$. These modifications are easy to understand qualitatively. When $\phi << 1$, the path of the reflected wave through the surface traverses many correlation lengths, and the roughness is effectively "averaged." When $\phi >> 1$, the surface appears "locally smooth" to the incident wave, and the specular reflection coefficient increases accordingly.

3.4.3 Discussion

The first and most obvious conclusion that can be reached is that no substantial difference exists between the optical properties of neutrons in metal capillaries and x-rays in glass capillaries. The effect of a

given surface roughness depends only on the critical angle and the penetration depth and not on whether neutrons or x-rays are being reflected. All of the statements in this report must therefore apply equally in both cases. However, no reason exists to expect that the surface roughness characteristics for metal and glass are at all similar.

With the results given in the previous section, the effects of surface roughness can be estimated rapidly. When $\phi \sim 1$ and $\Lambda = 0.1$, the specular reflection loss for most incident photons (or neutrons) is of the order of 1%. This is the source of the statement that glass capillary surfaces are necessarily smooth to 5Å. The logic used to arrive at this statement is somewhat indirect. Numerical simulation of the performance of capillary optics normally describes their actual performance well without incorporating surface roughness effects. However, a specular reflection loss any greater than 1% would clearly be important given the many reflections that are needed to pass through a capillary optical element. Consequently, it is concluded that the glass surfaces present inside real devices must be smooth to within 5Å. Although this logic is almost certainly correct, several qualifying statements are needed. The specified smoothness is required only when the roughness has a correlation length such that $\phi \sim 1$ or $\tau \sim P$. It is possible that the surface of real capillary devices is somewhat rougher, but has a dramatically different correlation length (P here is typically 10 μm). Thus, a small-wavelength roughness in excess of 5Å arising from the fundamental tetrahedral structure of the glass may be present with relatively little effect. In addition, the derivation of 5Å as a roughness limit used the assumption $\nu \sim 1$ since this is true for a great number of incident photons. However, these same photons are also subject to greater absorption since they are incident at nearly the critical angle. The photons that successfully transit a capillary device are probably weighted toward those photons that are incident with $\theta_i << \theta_c$ ($\nu << 1$). For these same photons, Eq. (3.8) predicts that a higher degree of roughness can be tolerated. Finally, it may not be true that any photon that undergoes a diffuse (non-specular) reflection is necessarily lost. If a substantial number of diffusely reflected photons are scattered in the forward direction, then their chances of successfully transiting the optic remain high, and the tolerable amount of surface roughness can be further increased.

An important point concerns the dependence of a capillary element's optical performance on the material's index of refraction in the presence of surface roughness. For a perfectly smooth surface, the highest possible index of refraction (highest electron density for glasses and highest coherent scattering length for neutrons) is desirable because it leads to the highest critical angle θ_c and therefore the highest transmission throughput. For a rough surface, however, a careful analysis must be performed. Remembering that the index of refraction for any material can be written $n = (1-\delta)^{1/2}$, the critical angle can be written $\theta_c = (\delta)^{1/2}$. Since the penetration depth also depends on δ as $D=1/k_I(\delta)^{1/2}$, the decrease in the specular reflection coefficient can be written

$$\Delta R=\nu\Lambda^2 = \sigma^2\theta_i k_i^2(\delta)^{1/2} \qquad (3.9)$$

Any increase in the material index of refraction, therefore, increases both θ_c and ΔR by the same factor. The total transmission of a capillary optical element should vary as θ_c^2, but also varies as $(\Delta R)^M$, where M is a potentially large integer representing the number of reflection that a wave undergoes as it transits the capillary. In conclusion, competing effects exist, and it is not clear that maximizing the quantity (1-n) is desirable for rough surfaces.

A final note concerns previous experimental investigations of surface roughness. Three studies have put forth values ranging from 38Å to 57Å for the surface roughness of the glass channels within a microchannel plate (MCP). The first of these (Kaaret et al. 1992) used optical profilometry and is not associated with any particular correlation length. The second (Fraser et al. 1993) uses surface roughness as

an adjustable parameter that is used to make a simulation of MCP reflection characteristics agree with observations. This results in a value of 50 ± 10 Å, again with no particular correlation length. The third study (Chapman et al. 1993) again determines surface roughness by forcing agreement between simulation and experiment and sets the surface roughness at $\sigma = 38$ Å with a correlation length of $\tau = 1.2 \pm 5$ μ. Two further experimental studies address capillary optics directly. Both of these (Xiao et al. 1993; MacDonald et al. 1993) also determine roughness as an adjustable parameter in a numerical simulation, and both find that incorporation of surface roughness is usually not needed to achieve good agreement. However, it is occasionally needed to match the observed characteristics of presumably rougher capillary devices. The first of these studies finds $\sigma = 12$ Å and $\tau = 60$ μ for one particular capillary device, while the second finds $\sigma = 20$ Å and $\tau = 0.6$ μ for another device. Note that these data generally support the nominal roughness in the neighborhood of 6 Å, but information on the correlation length is nonexistent or in wild disagreement.

3.5 Metal Capillaries

3.5.1 Introduction

The use of metal surfaces should greatly improve the transmission of neutron focusing devices based on glass polycapillary lenses because of the longer scattering lengths of metals compared to glass. We here report the results of our quantitative measurements of the neutron transmission of metal capillaries. Measurements were carried out using cold neutron beams and an imaging neutron detector. Metal capillaries obtained from commercial sources were studied as supplied and also as treated by chemical flow or electropolish techniques to compare the transmission performance as a function of the smoothness of the metal surface. The apparent reflectivities calculated from the experimental transmissions varied as a function of internal diameter and of capillary length, but were not sensitive to the various surface treatments studied here. None of the metal capillaries had reflectivities as good as the glass capillaries currently being used.

For neutron lenses, the material of choice is ^{58}Ni for the same reason that neutron guide tubes are made from ^{58}Ni. The large value for the coherent scattering length of ^{58}Ni means that the neutron wave penetrates into the surface less (smaller refractive index), and consequently, the chance that the neutron will be absorbed is reduced. This produces a greater critical angle, allowing transport of neutrons having greater angular divergence from the axis of the capillary. Nickel can easily be evaporated as a smooth coating on glass plates for use as neutron guide tubes. Capillaries made from natural nickel or enriched ^{58}Ni would have 2 or 3 times the neutron scattering length of glass capillaries. Stainless steel capillaries have a scattering length about 90% that of natural nickel and are readily available. Thus stainless steel capillaries should also be superior to glass capillaries. Stainless steel capillaries with inside diameters comparable to the first generation Kumakhov lenses can be purchased from commercial suppliers. The technology for producing smaller diameter metal capillaries probably has not been developed because of a lack of a perceived market.

The two key questions in using metal capillaries are 1) Is the inside surface of the capillaries smooth enough? and 2) Can metal capillaries be made with small enough inside diameters to allow short focal lengths? The second question is concerned more with the dimensions of a practical device whereas the first question is fundamental to whether the devices will work at all. In this work, we have chosen to address the first question by evaluating the performance of metal capillary tubes in transmitting neutrons.

At PNNL, we had previously examined the inside surfaces of commercially supplied capillary tubing for use in transporting small particles for direct-inlet mass spectrometry (Stoffels and Ells 1979). The

commercial tubing was not adequate, so we developed the capability of electropolishing small bore capillary tubes and evaluating the results by scanning electron microscopy. Our techniques were able to provide smooth, shiny bores with constant diameter throughout the length of the tube for tubes with inside diameters as small as 0.2 mm. As the first step in the development of metal capillary lenses, we wished to examine the performance of commercially supplied tubes compared to the electropolished tubes.

3.5.2 Experimental

Our goal was to compare the neutron transmission characteristics of stainless steel capillaries having various inside surface treatments. Capillary tubes with three types of internal surface preparation were obtained commercially (K-Tube Corp). The "K-Form" tubing is fabricated without exposing the interior to lubricants or mechanical drawing. This is the cheapest tubing. The "Matte-Draw" tubing uses floating plug drawing, which, according to the manufacturer's catalog, renders the weld line invisible and smooths interior surfaces. The "Brite-Draw" tubing is also produced by a floating plug process and is thought to have the best smoothness inside and outside. It is also the most expensive. The manufacturer claims that the Brite-Draw tubing looks as good as electropolished tubing. The tubing from this company was cut into lengths of 11 cm and 22 cm in our laboratories. In addition, we purchased capillary tubing from a second commercial vendor (MicroGroup, All-Tube Div., 7 Industrial Park Rd., Medway, Massachusetts 02053). This second batch of tubing was sent to another company (Stainless Micropolish, Inc., 1286 N. Grove Street, Anaheim, California 92806), which cut the tubing to the 11-cm and 22-cm lengths. This company then subjected half of these tubes to a chemical flow polish treatment.

At PNNL, we treated several of the K-Form tubes by the electropolishing technique described in work by Stoffels and Ells (Stoffels and Ells 1979). These included two different diameters, 23 gauge (0.318 mm I.D.) and 21 gauge (0.495-mm I.D.).

Most of the tubes tested for neutron transmission were either the 21-gauge or 23-gauge tubes. However, a few samples of the K-Form tubing having smaller inside diameters were tested, for example, 30 gauge (0.140-mm I.D.) and 26 gauge (0.241-mm I.D.). All of the Brite-Draw samples were 20 gauge (0.584-mm I.D.).

The transmission of neutrons was measured on a preliminary set of samples at the T13A diffractometer on neutron guide G5 at the Orphée reactor at Saclay, France, in Nov. 1994. Neutrons in the neutron guide were reflected off the 002 plane of a pyrolitic graphite crystal to give a scattered beam of neutrons with a wavelength of 4.74 Å (0.0036 eV). The divergence of this beam was measured in the scattering plane with an end-on 50-mm diameter ^{3}He proportional counter. The rocking curve was a Gaussian with s = 8.38 mrad (FWHM = 19.7 mrad). This beam was collimated by a cadmium sheet having a pinhole aperture of nominal diameter 0.35 mm. The vertical profile of the beam was measured after the pinhole with a video radiation detector. The divergence in the vertical direction was more complex, but could be approximated by a divergence with a FWHM of 20.8 mrad. The purpose of this collimator was to normalize the measurements for tubes of different radii to the same beam area and to reduce the background of neutrons traveling immediately outside the tube. The metal capillaries were mounted on the three-axis stage of the diffractometer and aligned with the neutron beam. This was done by adjusting the position of the capillary in both the horizontal and vertical directions until the intensity measured by the video radiation detector was maximized.

The video radiation detector consists of a video camera containing a CID imaging chip with a pixel size of 12 by 13.7 mm^2 and with a ^{6}LiF (n,α) converter film. The average intensity (T_{cap}) was evaluated by

integrating the number of counts in the pixels within a given radius. A computer model was used to estimate a simulated transmission (T_{sim}). The simulation model also gave the number of reflections (N). The simulations took into account the fact that for the set of tubes having an I.D. of 0.318 mm, the aperture did not restrict the full illumination of the tube, whereas for the set of tubes having an I.D. of 0.495 mm, the aperture prevented the tube from being fully illuminated (Mildner et al. 1995). This not only reduced the acceptance, but also reduced the number of trajectories that have a large number of reflections. The reflectivity was calculated from the expression

$$R = N(T_{exp} / T_{sim})^{1/N} \tag{3.10}$$

The results of this analysis are given in Table 3.4. For some of the samples, the measurements were made with one end of the capillary oriented toward the beam and then the other end toward the beam. This was done to test whether the electropolishing or chemical flow polishing techniques gave different results depending on the direction of the fluid flow during these polishing procedures. For the 0.318-mm-diameter tubes, the transmission was multiplied by $(350/318)^2$ to account for the fact that the aperture was larger than the tube.

The preliminary experiments did not show any significant trends regarding the performance of the inlet or outlet ends of the capillaries, so the two values were averaged. The uncertainties shown in Table 3.4 are the standard deviations based on the two measurements and are assumed to represent the reproducibility of duplicate measurements. Neither the electropolished nor the chemical flow polished samples gave any significant improvement over the untreated commercial samples. Moreover, none of the samples gave reflectivities of greater than 95%, which would be essential for use in a capillary lens.

A second set of experiments on a larger set of samples was performed at the NIST reactor in April, 1996. These were done on a cold neutron guide tube without the use of a diffractometer to provide a monochromatic beam. Consequently, a distribution of neutron energies was in the beam, but the available neutron flux was much higher than in the first experiment. The average neutron energy corresponded to a wavelength of 6 Å (0.0023 eV). The energy distribution peaked at 5 Å (0.0033 eV). The angular divergence of the beam was given by the supermirror of the guide (3.46 mrad/Å). Note that thermal neutrons are typically about 0.025 eV. The neutron flux was about 10^9 n/cm^2-s. Individual capillaries were clamped in an aluminum holder mounted on a computer controlled stage with angular adjustments in two dimensions. The front of the holder was shielded with a flexible polymer sheet loaded with ^{6}Li. This sheet had a pinhole approximately equal to the size of the tubing. A small collar of parafilm wax was attached outside of the downstream end of the tube. Any neutrons that leaked past the pinhole collimator outside the capillary were scattered by the wax collar. This arrangement provided excellent contrast between neutrons traveling within the capillary and background neutrons when using the position-sensitive CID camera. Images with sufficient statistical accuracy could be obtained with 20-second count times.

Table 3.4. Transmission and Reflectivities of Stainless Steel Capillaries Measured in Preliminary Experiment

Sample ID	Diameter I.D. (mm)	Length (mm)	Transmission (exp)	Reflectivity Eq. 2.1	Average Reflectivity
Electropolished					
K23R inlet	0.318	110	0.38	0.78	0.76
K23R outlet	0.318	110	0.33	0.74	±0.03
K21R inlet	0.495	110	0.58	0.86	0.88
K21R outlet	0.495	110	0.63	0.90	±0.03
K21R inlet	0.495	220	0.31	0.78	0.76
K21R outlet	0.495	220	0.25	0.73	±0.04
Chem. Polished					
K23R inlet	0.318	110	0.36	0.77	0.72
K23R outlet	0.318	110	0.25	0.67	±0.07
K23R inlet	0.318	220	0.21	0.80	0.78
K23R outlet	0.318	220	0.16	0.76	±0.03
K21R inlet	0.495	110	0.43	0.73	0.74
K21R outlet	0.495	110	0.45	0.75	±0.01
K-Form[a]					
K23R	0.318	110	0.31	0.72	
K23R	0.318	220	0.13	0.73	
K21R	0.495	110	0.55	0.84	
K21R	0.495	220	0.097	0.56	

(a) Untreated - as supplied

In measuring the transmission of a capillary tube, the average neutron flux with the tube was compared with the neutron flux without the tube. First, an image of the neutron beam without any collimation was obtained and stored in the computer as a reference image. Then, the pinhole collimator and capillary tube were mounted in place. The neutron count rate within a specified region corresponding to the beam spot was optimized by adjusting the left-right and up-down angle of the capillary in steps of 0.05 degrees. An example of a detailed rocking curve in the horizontal plane is shown in Figure 3.7.

Once the optimum position was determined, the image of the neutron spot was obtained. The average count rate per pixel over a circular region with a diameter of 30 (sometimes 40) pixels was calculated by the imaging software. The average count rate over this region was compared with the average count rate over the same region in the no-capillary reference image. The ratio of these average count rates was the transmission.

The transmission (T_{exp}) of the metal capillaries can be converted to a reflectivity that represents the smoothness of the inner surface. Reflectivity (R) is a measure of the probability that a neutron striking the surface at an angle less than the critical angle will be reflected rather than absorbed. The transmission and reflectivity are related by the number of reflections (N) that the neutron must undergo to transit the capillary. For glass capillaries where the reflectivities are close to one, the approximation given in Eq. 3.11 is valid.

$$T_{exp} = \langle R^N \rangle \approx R^{\langle N \rangle} \tag{3.11}$$

One can then calculate the reflectivity using a calculated mean value ($\langle N \rangle$) of the number of reflections where $\langle N \rangle$ is found from Eq. 3.12. The length of the capillary is L and the diameter is D.

$$\langle N \rangle = (8/3\pi)(\theta_d L/D) \tag{3.12}$$

These equations are valid when the beam divergence (θ_d) is less than the critical angle. The beam divergence in this experiment was 8.35 mrad, whereas the critical angle for stainless steel at the peak wavelength (6 Å) was 8.82 mrad.

The reflectivities for the capillaries in this work were not close to 1.0, so a more detailed analysis was required. The more exact expression relating the transmission and reflectivity is given in Eq. 3.13

$$T_{exp} = \Sigma\, t(n)\, R^n \tag{3.13}$$

where n is an integral number of reflections and t(n) is the relative fraction of the transmitted trajectories that have exactly n reflections. These relative fractions increase linearly with the order of reflection up to some value beyond which it will fall because the cylindrical channel is not fully illuminated. The range over which this linearity exists is proportional to the length and inversely proportional to the diameter of the capillaries. The calculated distributions of the relative probabilities of individual numbers of reflections are shown in Figure 3.8 for 110-mm-long capillaries with the diameters tested in this work. A similar plot for 220-mm-long capillaries is shown in Figure 3.9.

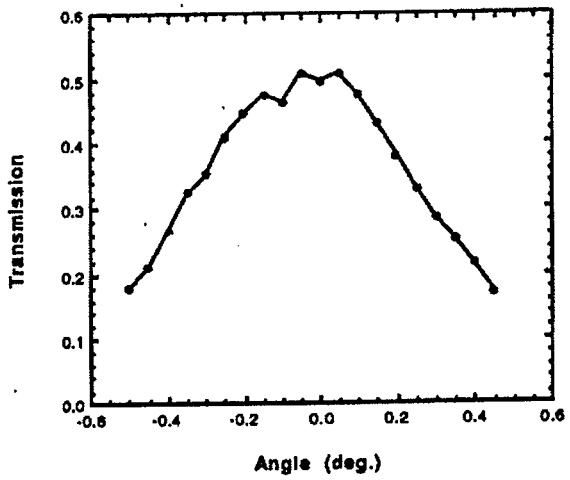

Figure 3.7. Neutron Transmission as a Function of the Horizontal Angle of a Capillary Relative to the Beam Axis. This is based on a circular beam spot area of 40-pixel diameter.

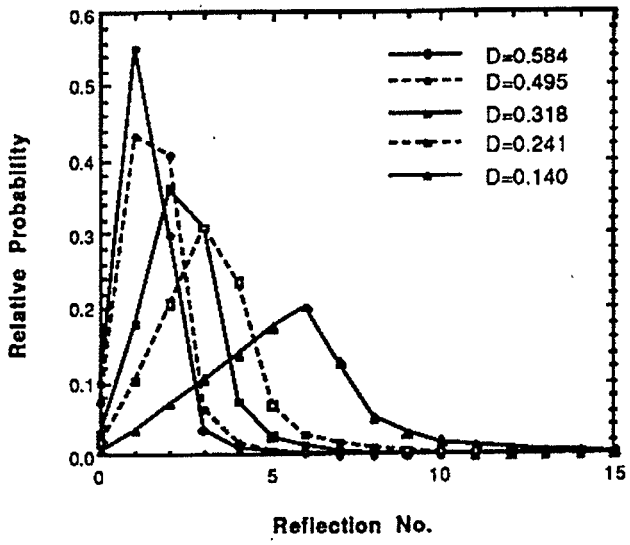

Figure 3.8. Normalized Relative Probabilities of Trajectories Having a Specific Number of Reflections for 110-mm-Long Capillaries Having the Inside Diameters Indicated

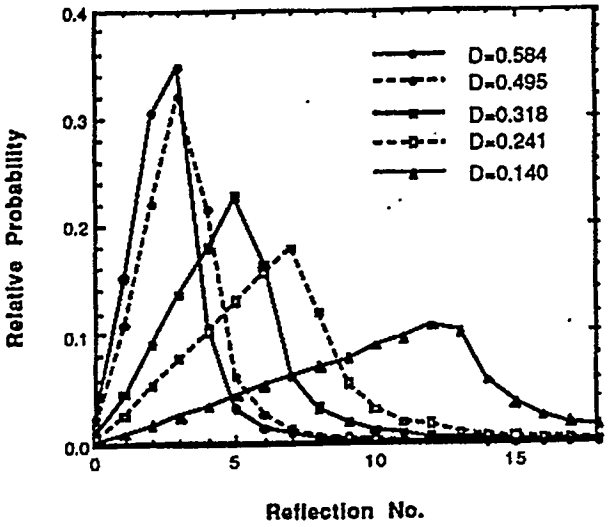

Figure 3.9. Normalized Relative Probabilities of Trajectories Having a Specific Number of Reflections for 220-mm-Long Capillaries Having the Inside Diameters Indicated

The reflectivity is determined by finding a value of R that reproduces the experimental transmission. In this case, the analogous expression to Eq. 3.12 is the effective number of reflections $\underline{n}$ given in Eq. 3.14.

$$\underline{n} = \Sigma n \cdot t(n) \tag{3.14}$$

The <N> calculated from Eq. 3.12 and the $\underline{n}$ calculated from Eq. 3.14 for the various lengths and diameters used in this work are shown in Table 3.5.

Table 3.5. Values of Mean <N> and Effective n Number of Reflections for the Stainless Steel Capillaries Used in this Work

Length (mm)	Diameter (mm)	<N> Eq. 2.3	n Eq. 2.5
110	0.140	5.569	5.512
110	0.241	3.235	3.229
110	0.318	2.452	2.444
110	0.495	1.575	1.573
110	0.584	1.335	1.340
220	0.140	11.138	10.636
220	0.241	6.470	6.384
220	0.318	4.903	4.870
220	0.495	3.150	3.138
220	0.584	2.670	2.667

The results for the experimental transmissions and the reflectivities calculated by Eq. 3.11 and 3.13 are given in Table 3.6.

Table 3.6. Transmission and Reflectivities of Stainless Steel Capillaries

Sample Id[4]	Diameter I.D (mm)	Length (mm)	Transmission (exp)	Reflectivity Eq. 3.11	Average Reflectivity	Reflectivity Eq. 3.13	Average Reflectivity
Electropolished							
EP48	0.318	110	0.48	0.741	0.808	0.715	0.792
EP53	0.318	110	0.72	0.875	±0.095	0.868	±0.108
EP61	0.318	220	0.28	0.771		0.734	
K21R 9/19/95	0.495	110	0.93	0.955	0.968	0.954	0.963
K21R 9/26/95	0.495	110	0.96	0.987	±0.017	0.974	±0.010
K21R 9/27/95	0.495	110	0.94	0.961		0.961	
Chem. Polished							
K23R-CP	0.318	220	0.28	0.771		0.734	
K23R-CP-MG	0.318	110	0.63	0.828	0.826	0.817	0.814

Sample Id[a]	Diameter I.D (mm)	Length (mm)	Transmission (exp)	Reflectivity Eq. 3.11	Average Reflectivity	Reflectivity Eq. 3.13	Average Reflectivity
K23R-CP-MG	0.318	110	0.62	0.823	±0.004	0.810	±0.005
K23R-CP-MG	0.318	220	0.33	0.798		0.768	
K21R-CP	0.495	110	0.86	0.909		0.906	
K21R-CP	0.495	220	0.58	0.841		0.829	
K21R-CP-MG	0.495	110	0.92	0.948	0.958	0.948	0.958
K21R-CP-MG	0.495	110	0.95	0.968	±0.014	0.968	±0.014
K21R-CP-MG	0.495	220	0.51	0.808		0.789	
K-Form							
K26R	0.241	110	0.26	0.659		0.603	
K23R	0.318	110	0.74	0.884	0.840	0.879	0.829
K23R	0.318	110	0.57	0.795	±0.063	0.779	±0.071
K23R	0.318	220	0.24	0.747		0.702	
K23R-MG	0.318	110	0.63	0.828		0.817	
K23R-MG	0.318	220	0.33	0.798		0.768	
K21R	0.495	110	0.87	0.915		0.913	
K21R	0.495	220	0.60	0.850		0.839	
K21R-MG	0.495	110	0.94	0.961	0.965	0.961	0.965
K21R-MG	0.495	110	0.95	0.968	±0.005	0.968	±0.005
K21R-MG	0.495	220	0.55	0.827		0.812	
Matte-Draw							
M21R	0.495	110	0.90	0.935	0.925	0.934	0.924
M21R	0.495	110	0.87	0.915	±0.014	0.913	±0.015
M21R	0.495	220	0.48	0.792		0.771	
Brite-Draw							
B20R	0.584	110	0.99	0.992	0.977	0.993	0.978
B20R	0.584	110	0.95	0.962	±0.021	0.962	±0.022
B20R	0.584	220	0.50	0.771		0.749	

(a) MG = MicroGroup, all others = K-Tube Corp., San Diego, California

3.5.3 Discussion

The quantity and quality of the data obtained in the second set of experiments were much superior to the preliminary experiments. In cases where data were obtained on duplicate samples, the results were averaged, and the standard deviation of the distribution is shown as the uncertainty of the average value. For the eight cases with duplicate measurements, the average value of the fractional uncertainty was about 4%. The first observation to make about the data in Table 3.6 is that when the reflectivity is high ($R > 0.9$), the approximate expression Eq. 3.11 and the more exact expression Eq. 3.13 give the same result. As the reflectivity decreases below $R = 0.9$, the approximate expression overestimates the reflectivity. The second observation is that in every case, reflectivities obtained for the 220-mm samples were less than the reflectivities obtained for the equivalent 110-mm samples. In principle, the reflectivity should be independent of the length of the capillary. It is possible, however, that the longer capillaries were not held as straight as the shorter capillaries so that the observed result is due to slight bending of the longer capillaries. A third observation is that the measured reflectivities seem to depend on the diameter of the capillary such that larger diameters give higher values.

The principle goal of this work was to evaluate the various surface treatments with respect to smoothness. For this comparison, we discuss only the data for the 110-mm capillaries and treat the different diameter samples separately. For the 23-gauge (0.318-mm) samples, the reflectivities are listed in Table 3.7. Within the uncertainties due to reproducibility, no preferred surface treatment appears to exist for this set of capillaries.

Table 3.7. Reflectivities Based on Eq. 3.13 for 110-mm-Length and 0.318-mm-Diameter Tubes

Surface Treatment	Reflectivity
Electropolish	0.792 ± 0.108
Chemical flow polish	0.814 ± 0.005
K-Form	0.829 ± 0.071

The reflectivities for the 21-gauge (0.495-mm) samples are listed in Table 3.8. In this group, the electropolished samples from PNNL, the chemical flow polish samples supplied by MicroGroup, and the K-Form samples from MicroGroup all perform equally well. In view of the extra cost associated with the electropolishing and chemical flow polishing, these treatments offer little benefit. For purposes of neutron transmission, the cheapest grade of commercial material seems to be comparable to more expensive treatments.

Table 3.8. Reflectivities Based on Eq. 3.13 for 110-mm-Length and 0.495-mm-Diameter Tubes

Surface Treatment	Reflectivity
Electropolish	0.963 ± 0.010
Chemical flow polish	0.906
Chemical flow polish - MG	0.958 ± 0.014
K-Form	0.913
K-Form - MG	0.965 ± 0.005
Matte-Draw	0.924 ± 0.015

The material with the highest reflectivity among the samples measured here was the Brite-Draw sample with a reflectivity of 0.978 ± 0.022. However, this material was not available in diameters less than 0.584 mm. In view of the observed trend of increasing reflectivity with increasing diameter, this good performance may be due more to the larger diameter than to the improved (and expensive) surface treatment.

As a demonstration of the use of metal capillaries to transmit neutrons, we bundled 10 of the 0.318-mm-diameter, 110-mm-long K-Form tubes and placed them in the neutron beam. The image obtained with the video radiation detector is shown in Figure 3.10. No attempt was made to bend the tubes to form a focus. The bright spots in the image are simply the transmitted neutrons from the individual tubes in the bundle.

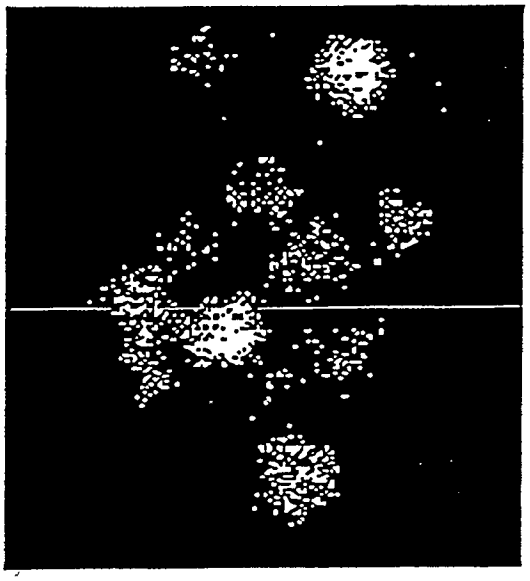

Figure 3.10. Image of Bundle of 10 Metal Capillary Tubes

3.5.4 Conclusions

The transmission and reflectivities of stainless steel capillary tubes having a variety of surface treatments have been measured with cold-neutron beams. The more expensive drawing processes (Matte-Draw and Brite-Draw) and surface treatments (electropolishing and chemical flow polishing) do not provide an obvious improvement in the measured reflectivities. Reflectivities of greater than 0.95 can be obtained from the cheapest grade (K-Form) tubing. However, the reflectivity appears to get worse when going to smaller diameter tubing. This is unfortunate as smaller diameter tubing is desired to construct more compact focusing devices. The successful neutron lenses made from glass polycapillaries have reflectivities of about 99%. It remains to be seen whether metal coatings on glass substrates might provide equally good performance.

3.6 Efficiency Calculation

A careful calculation of transmission efficiency E is required to properly optimize a neutron optical system for use in applications. The overall efficiency of a neutron lens can be written as the product of five independent efficiencies:

$$E=(T_r T_b)(A_p A_x A_r) \tag{3.15}$$

The first two of these efficiencies ($T_r T_b$) account for losses that occur during the neutron reflection process. Three additional efficiencies ($A_p A_x A_r$) are needed to account for the total open area ratio of a capillary neutron lens. The following discussion describes these six efficiencies generally; a subsequent section contains an efficiency calculation for a particular lens intended for neutron capture therapy.

Reflection losses in a capillary lens occur when a neutron fails to be properly reflected due to nonidealities (T_r) or fails to be reflected because of capillary bending (T_b). The reflection efficiency T_r results from the numerous reflections that neutrons must make as they traverse a capillary within the lens. Although the probability of absorption or diffuse scattering at each reflection is roughly one percent or less, the accumulated result can be an efficiency that is substantially less than one but not less than 0.5 for typical lens lengths (Xiao et al. 1993). The bending efficiency T_b depends on the severity of the curvature for a particular capillary. For lenses in which the capillary curvature violates the limit given in Eq. (2.6), the bending efficiency becomes substantially less than one (Kumakov and Komarov 1990). Ordinarily, lenses are designed so this does not occur.

The open area ratio of a neutron lens describes the fraction of its front surface that is composed of useful capillary area. The unusable fraction of the lens surface is composed of the glass used to construct the polycapillary fibers and the spaces between the polycapillary fibers. The total open-area ratio for the entire lens acts mathematically as an efficiency and is the product of the open-area ratio for a polycapillary fiber, A_p, and the fractional area taken up by the polycapillaries, $A_x A_r$. The open area ratio for the polycapillaries used to construct lenses is generally between 0.35 and 0.55. A typical value would be 0.5. The fact that the polycapillaries take up less than 100% of the lens surface results from two separate causes. First, polycapillaries of constant cross section can take up no more than $A_x=R_x^2/R_e^2$ of the surface area of a lens that narrows from an entrance radius of R_e to an exit radius of R_x. This "shrinkage" open area A_x is less than one only for half-barrel lenses. A "residual" open area ratio results from the fact that it is impossible to pack the

polycapillaries perfectly even at the back (exit) surface of the lens. The resulting "residual" open area A_r typically has the value 0.75.

Combining all of the above efficiencies for a lens built with a maximum curvature satisfying Eq. (2.6) yields

$$E \sim 0.19 \, (R_x^2/R_c^2) \tag{3.16}$$

This formula can be used to help calculate the neutron delivering power of a neutron optical system of arbitrary design.

4.0 PNNL's Applications

This section describes three applications for capillary optics technology that PNNL has explored. These applications are not connected otherwise. The applications can be summarized as follows:

- We have proposed the use of a capillary neutron lens to construct a "neutron telescope" for remote determination of the direction and strength of distant neutron sources. The lens allows the use of a small neutron detector with a correspondingly low background count rate.
- We have experimentally demonstrated that a capillary x-ray lens would permit more rapid sample analysis via the technique of powder diffractometry. The lens significantly increases the x-ray flux striking the sample.
- The use of a neutron lens has been proposed and theoretically analyzed for medical neutron radiotherapy. Such a technology may someday allow economically practical treatment of brain tumors.

4.1 Neutron Telescope

4.1.1 Introduction

The detection of neutrons has long been one of the major techniques for distinguishing nuclear weapons or nuclear weapons material from conventional weapons or material. The emission of neutrons from nuclear weapons material is primarily due to spontaneous fission of even mass isotopes of Pu. The neutron spectra from spontaneous fission have average energies of about 2 MeV. However, the spectrum is usually degraded by the presence of moderating materials in the vicinity of the Pu. The typical neutron detector used for detecting such sources has been one or more gas proportional counters containing BF_3 or ^3He embedded in a moderating material such as polyethylene. The fast neutrons in the degraded energy spectrum are moderated to thermal energies by the polyethylene and then captured by ^{10}B or ^3He in the proportional counters. The presence of the polyethylene moderator dramatically increases the efficiency for detecting the neutrons.

To obtain directional information from a moderated neutron detector, detectors have been built with cadmium or other neutron absorbing material surrounding the detector on all sides except the side facing the source (East and Walton 1969). An additional moderator has been placed outside the cadmium to thermalize the fast neutrons so they can be more efficiently absorbed. The net result is a detector package that is large and heavy. If the detector is used in a location with concrete floors or other nearby scattering material, it is difficult to pinpoint the location of the neutron source.

In contrast to conventional approaches, we use a philosophy similar to that presented by Vanier et al. for building a directional neutron detector (Vanier et al. 1995). The basic concept is to place a neutron detector that is sensitive only to thermal neutrons inside a thermal neutron shield (cadmium box) and to restrict the field of view by a collimating array of a thermal neutron absorber. The angular resolution can be adjusted to any desired value by the use of collimating arrays with different ratios of length to width. We avoid the use of any moderating material inside the thermal neutron shield and depend only on detecting the thermal neutrons produced directly by the source. The resulting detector is much smaller and lighter than the corresponding moderated detectors and is thus easier to shield. A low detector background is essential for

this approach because we detect only the thermal neutrons produced directly from the source and are insensitive to a large fraction of the total neutron signal.

Conventional wisdom has assumed that thermal neutrons are quickly scattered and rapidly lose all directional information. However, the work of Vanier, Forman, and Selcow (1995), Monte Carlo calculations, and our laboratory experiments have borne out the fact that a significant fraction of the thermal neutrons will travel straight paths before being scattered or absorbed by air. If a 1 m^2 detector has a background of 0.4 cps, we predict that a neutron source of 10^5 n/s could be detected at a distance of 50 m in a counting time of 50 minutes. This estimate is based on the additional assumptions that 10% of the neutrons leaving the source are at thermal energies, the mean free path of a thermal neutron in dry air is 22 m, the detection efficiency of thermal neutrons is 100%, and detection is confirmed when the signal is twice the statistical uncertainty.

It has been proposed that a capillary neutron lens could gather the neutron radiation incident over an extended area, focusing it down onto a narrow "spot" where a small neutron detector could be located. Figure 4.1 shows a schematic of this "neutron telescope." Since the background count rate in a neutron detector is proportional to its area, the smaller detector would have a far lower background count rate. The lens might therefore allow more accurate measurements to be made more quickly.

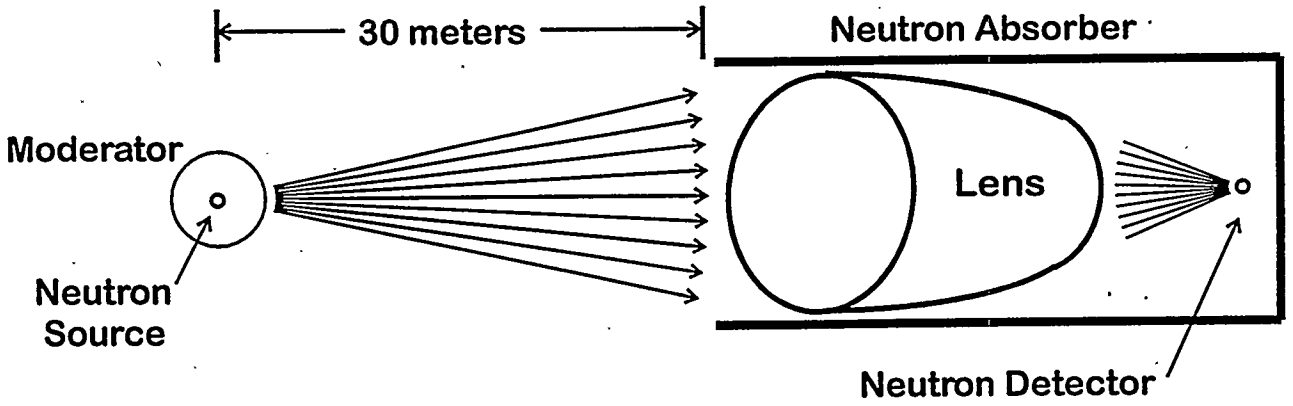

Figure 4.1. Schematic Diagram of the Proposed "Neutron Telescope"

Most ordinary neutron detectors are sensitive to neutrons with a range of energies and from a variety of directions. The lens, however, focuses only those neutrons from a specific direction and with thermal energies. This characteristic has both good and bad ramifications. The neutron detector at the heart of the neutron telescope can be constructed and shielded in such a way that it, too, is sensitive to only certain neutrons. This will result in a far lower background rate than even that predicted on the basis of the detector's area. However, as we calculate below, the detector's signal count rate may become so low that long measurement times are required.

We calculate the signal rate by assuming that a neutron source inside a 10-cm-radius moderating sphere results in the emission of 10^4 neutrons/second in random directions. It can be shown that the signal strength is independent of the source-telescope separation distance provided that the telescope is not "looking" at a region that is larger than the moderating sphere. Since the critical angle for neutrons

thermalized to room temperature in a glass capillary is 2×10^{-3} radians, we shall choose the largest distance possible before signal strength begins to decrease. This distance, 50 m, is the distance at which the moderating sphere completely "fills" the region from which the neutron telescope can gather neutrons. (We neglect the fact that at this distance, some fraction of the emitted neutrons will scatter from air molecules between the source and the telescope.) Under these conditions and assuming a lens radius of 10 cm, the solid angle collection efficiency of the telescope will be roughly 10^{-6}. Assuming a further efficiency of 10 percent for the lens itself, the expected signal rate becomes 3.6 counts/hour. Even at this level, the signal may well be above the background.

Although this count rate is low, it is still remarkable that the measurement can be achieved at all using a device that is no bigger than a hobbyist's optical telescope. The same measurement without a capillary lens would require a panel with an area of roughly 1 square meter and have no directional sensitivity. In other words, the panel-based measurement could tell that a neutron source was *somewhere* within 50 meters, but not where. As with x-ray diffractometry, the neutron telescope will benefit directly from continuing improvements in capillary lens technology. For example, a lens identical to the one assumed above but constructed from ^{58}Ni would have a signal 4 time larger than the value given above. Further increases in signal strength would be likely to occur should monolithic lens construction technology be adopted.

To better understand the characteristics and benefits of directional thermal neutron-only measurement, we constructed several devices to allow investigation of this topic. We here describe a narrow-field-of-view thermal neutron detector that we have constructed. Its angular resolution and sensitivity as a function of distance from a source are discussed. We describe the results of tests that were performed to determine the effect of moderating material in various configurations near the actual fast neutron source.

4.1.2 Narrow-Field-of-View Detector

Two similar detector systems were tested, one using BF_3 counter tubes and the other using ^{3}He counter tubes.

^{3}He Detector

The narrow-field-of-view ^{3}He neutron counter is shown in Figure 4.2. The ^{3}He proportional counter tubes were 2.54-cm diameter by 35.6-cm active length filled with 4 atm of ^{3}He. The tubes were arranged in two rows with 11 tubes in the front row and 12 tubes in the back row. The center-to-center spacing between tubes within a row was 3.46 cm whereas the center-to-center spacing between rows was 2.86 cm. The counter tubes were held in place by two 0.159-cm-thick stainless steel sheets with holes cut at the desired locations. The counter tubes and the stainless steel frame were contained in a 5-sided cadmium box made from 0.076-cm-thick sheets. The dimensions of the box were 48.9 by 45.1 by 12.7 cm^3. The collimating array was made from 0.076-cm-thick cadmium sheet rolled into 2.54-cm-diameter tubes that were 10.16 cm long, which gave a length-to-diameter ratio of 4. The active area of the counter tubes was 40.6 by 35.6 cm^2, and this area was filled with the cadmium tubes arranged perpendicular to the axes of the counter tubes. The extra open space not occupied by the collimating array was covered with cadmium sheet so that thermal neutrons could only reach the counter tubes by traveling within the open space of the collimating array.

The field-of-view for thermal neutrons was defined as the angle from the axis of the cadmium tube at one end of the tube to the wall at the other end of the tube as shown in Figure 4.3. With this definition, the field-of-view is 7.12 degrees. Neutrons whose paths lie within this field-of-view should have 50% or greater

probability of reaching the interior of the detector. Neutrons at angles greater than 7.12 degrees can also be detected, but with decreasing efficiency up to the limit at 14.0 degrees. The collimating array was assembled by close-packing the cadmium tubes. The space between tubes was left open, but restricted the field-of-view more than the tubes themselves. The open area of the collimating array was calculated to be 89%.

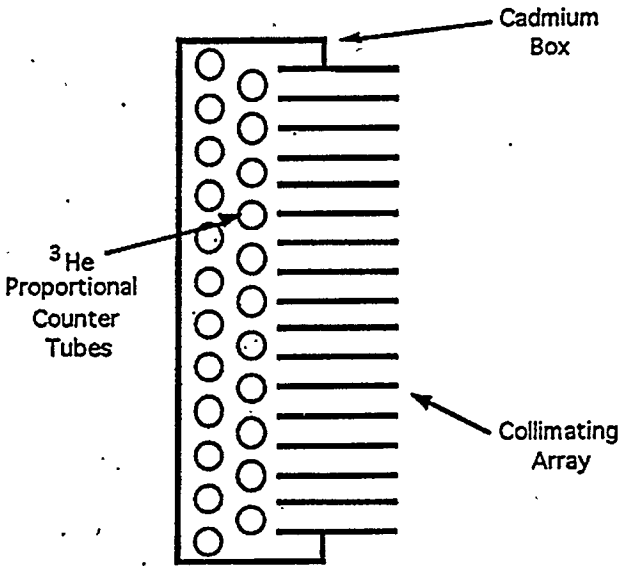

Figure 4.2. Schematic Drawing of Narrow-Field-of-View Neutron Detector

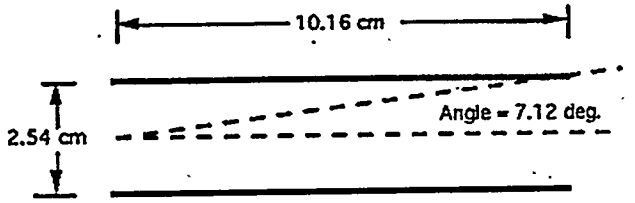

Figure 4.3. Schematic Representation of Field-of-View as Defined in the Text

BF_3 Detector

The narrow-field-of-view detector using 2.54-cm-diameter BF_3 counter tubes was similar in size and construction to the ^{3}He detector described above. Only 21 tubes were used. They were arranged in two rows with 10 tubes in the front row and 11 tubes in the back row. The collimating array was the same set of cadmium tubes as used with the ^{3}He detector. The BF_3 detector was actually constructed before the ^{3}He detector and was used for the initial experiments. Unfortunately, the BF_3 tubes exhibited poor pulse-height resolution and excessive noise. However, the data obtained with the BF_3 detector encouraged us to proceed with the more reliable ^{3}He detectors as soon as the tubes became available.

4.1.3 Angular Resolution

Our first experimental test was to demonstrate that the narrow-field-of-view detector was capable of locating a thermal neutron source with the angular resolution expected from the design of the collimating array. A source of thermal neutrons was created by placing a small PuBe neutron source (1.58 by 10^5 n/s) centered behind a block of polyethylene 5.08-cm thick by 30.5-cm square. The BF_3 detector was placed 180 cm from the source. Both the source and the center of the neutron detector were at 119 cm above the floor. With this geometry, the field-of-view of the detector included the entire 30.5-cm square face of the polyethylene moderator from which thermal neutrons were emitted.

To obtain the angular resolution, the neutron source was held fixed, and the detector was rotated about its vertical midpoint of the counter array at a constant distance from the source. The count rate as a function of angle is shown in Figure 4.4 where 0 degrees is defined as the condition where the face of the neutron counter is parallel to the 30.5-cm-square face of the polyethylene. The data were obtained as 100 s counts at 5 degree intervals near 0 degrees and at 10 degree intervals beyond 30 degrees. The prominent peak at 0 degrees shows that this detector does have the angular response expected for the collimating array employed here.

The angular response of the ^{3}He detector was also measured in the same manner as for the BF_3 detector. In this case, the source was placed between two polyethylene blocks, each 5.08-cm thick by 30.5-cm square with the detector at a distance of 3.05 m. The angular response data are shown in Figure 4.5. Again a prominent peak was observed. The peak-to-tail ratio for the ^{3}He detector is even better than for the BF_3 detector.

Proof that the peak at 0 degrees in the data from the ^{3}He detector was due to thermal neutrons was obtained by placing a sheet of cadmium over the collimating array with the detector oriented at 0 degrees. The net count rate dropped from 19.2 ± 0.2 cps to 4.7 ± 0.2 cps. The count rate with the cadmium cover at 0 degrees was comparable to the uncovered count rate at angles greater than 30 degrees.

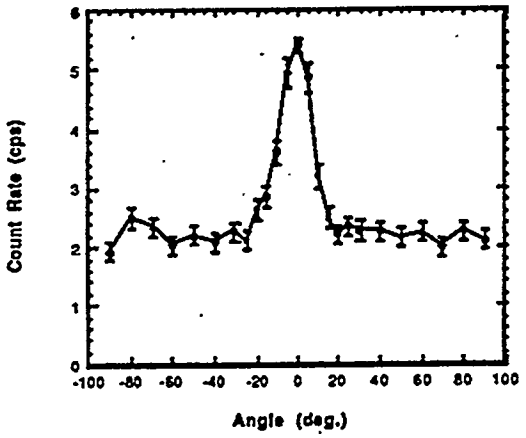

Figure 4.4. Neutron Count Rate Versus Detector Angle for BF_3 Detector 180 cm from Source. Room background of 0.35 ± 0.06 cps has been subtracted.

Additional confirmation that the peak was due to thermal neutrons was obtained by measuring the ratio of count rates when the ^{3}He detector was oriented at 0 degrees and at 90 degrees, but using a bare neutron source without moderation. At 0 degrees, the count rate was 2.9 ± 0.2 cps while at 90 degrees, the count rate was also 2.9 ± 0.2 cps.

The tails of these angular response curves have higher count rates than we initially expected. This could be caused either by epithermal neutrons that penetrate the Cd shield and are captured in the ^{10}B or ^{3}He without thermalization or by fast neutrons that penetrate the Cd shield and cause elastic scattering. With ^{3}He, elastic scattering of neutrons above 250 keV begins to exceed the discriminator threshold for our neutron counter. Because of different kinematics, elastic scattering does not interfere with BF_3 counters until the neutron energy exceeds 2.5 MeV.

The angular response test was repeated with the ^{3}He detector at 3.05 m with a single channel analyzer set to accept only those pulses falling in the full energy peak in the pulse-height spectrum. Thus, only neutrons with energy greater than 1.0 MeV could contribute to the neutron count rate by elastic scattering on ^{3}He. No difference was observed in the ratio of counts at 0 degrees to counts at 30 degrees for the data taken with the single channel analyzer and the data taken with acceptance of all neutron pulses. We assume that the number of neutrons above 1.0 MeV from our moderated PuBe source is significantly less than the number above 250 keV. The data therefore indicate that elastic scattering of fast neutrons within the ^{3}He tubes does not contribute significantly to the observed count rates.

The count rate at the detector orientation of 90 degrees could be due either to fast neutrons penetrating the shield or thermal neutrons scattering around the room and entering the detector through the collimating array. To distinguish these two possibilities, we used the BF_3 detector at 3.05 m from the source and compared the count rates with and without 5.08 cm of additional moderator on the 5 sides of the cadmium box. With the detector oriented at 90 degrees to the source and no extra moderator, the net count rate was 1.61 ± 0.07 cps. With the extra moderator, the count rate dropped to 0.77 ± 0.04 cps. However, the background with the extra moderator increased from 0.35 ± 0.06 cps to 0.77 ± 0.04 cps, indicating that the extra moderator had eliminated the detection of fast neutrons from the source, and all the remaining counts were due to cosmic rays.

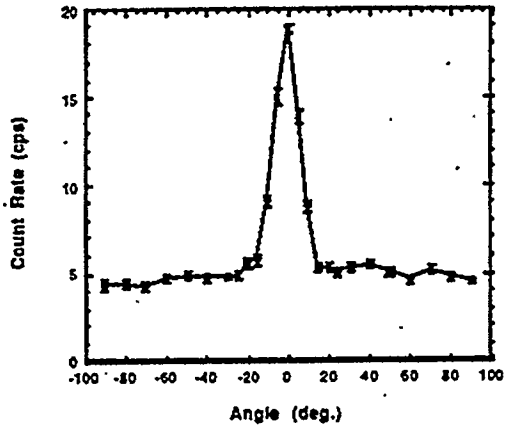

Figure 4.5. Neutron Count Rate Versus Detector Angle for ^{3}He Detector 3.05 m from Source. Room background of 0.32 ± 0.01 cps has been subtracted.

We also tested the effect of room-scatter neutrons using the ^{3}He detector at 3.05 m from the source. With the detector oriented at 90 degrees to the source, the count rate was measured with and without a cadmium sheet covering the collimating array. Without the cadmium cover, the net count rate was 4.37 ± 0.22 cps, whereas with the cadmium cover, the count rate was 4.66 ± 0.22 cps. This test plus the earlier test with the extra polyethylene moderator showed that room scatter of thermal neutrons did not contribute to the count rate when the detector was oriented away from the source.

4.1.4 Sensitivity vs Energy Spectrum

We were not able to measure the energy spectrum of the neutron source directly. However, we did vary the ratio of thermal neutrons to fast neutrons by changing the thickness of the moderator in front of the source. The source configuration consisted of a 5.08-cm-thick slab of polyethylene moderator behind the source and a variable thickness of moderator in front of the source. Monte Carlo calculations showed that the thermal neutron flux leaving the moderator peaks at roughly 5-cm thickness. As additional moderator is placed in front of the source, the thermal flux decreases because of increased absorption of thermal neutrons within the moderator.

A plot of the neutron count rate as a function of moderator thickness obtained with the ^{3}He detector at 0 degrees and at 30 degrees is shown in Figure 4.6. When the detector is oriented at 0 degrees to the source, it is primarily measuring the thermal flux. When the detector is oriented at 30 degrees, it is primarily measuring epithermal and fast neutrons that can penetrate the cadmium shield. The 0-degree count rate peaks as expected at about 5-cm thickness, whereas the 30-degree count rate falls off monotonically with increasing moderator thickness.

As shown in Figure 4.7, the 0-degree to 30-degree ratio reflects the relative changes in the thermal to fast component of the neutron source energy spectrum as the moderator thickness was changed. Thus, the ratio of neutron count rates at 0 degrees to 30 degrees can be used as a crude measure of the neutron energy spectrum. In addition, the fact that the 0-degree to 30-degree ratio is greater than 1.0 over this range of moderator thicknesses shows that the source location capability of the narrow-field-of-view detector is excellent even for a variety of source energy spectra.

4.1.5 Sensitivity vs Distance

To demonstrate that good angular resolution could still be obtained at greater distance, the source was moved into a hallway, and the BF_3 detector was located 12.2 m away. Data were obtained only at 0 degrees and 30 degrees as these angles represent the source within the field-of-view and the source outside the field-of-view. The same experiment was repeated with the ^{3}He detector. Even at 12.2 m, the net count rate at 0 degrees is about 3 times the net count rate outside the field of view (30 degrees) as shown by the data in Table 4.1.

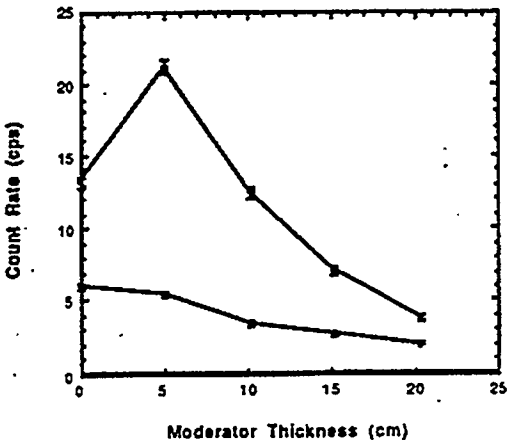

Figure 4.6. ^{3}He Detector Count Rate at 3.05 m from Source as a Function of Moderator Thickness at Source. The upper curve applies for a detector orientation of 0 degrees. The lower curve applies for a detector orientation of 30 degrees.

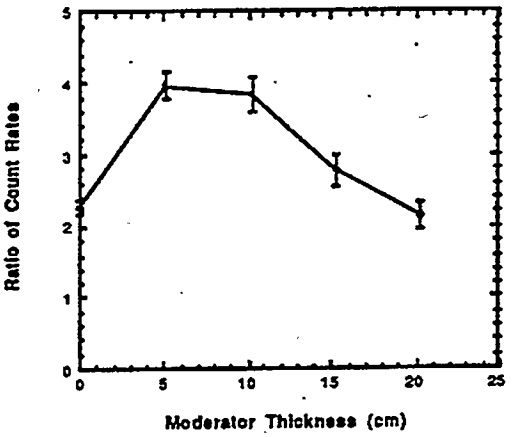

Figure 4.7. Ratio of Neutron Count Rates with Detector Oriented at 0 Degrees and 30 Degrees. Source to detector distance was 3.05 m.

Table 4.1. Ratio of Neutron Count Rates with Detector Oriented at 0 Degrees and 30 Degrees. Source to detector distance was 3.05 m.

Detector	Distance	cps (0 degrees)		cps (30 degrees)		Ratio	
BF_3	1.80	5.40	±0.10	2.61	±0.11	2.07	±0.09
BF_3	3.05	4.79	±0.16	1.61	±0.07	2.98	±0.16
BF_3	12.2	0.73	±0.05	0.18	±0.05	4.16	±1.13
^{3}He	3.05	19.20	±0.20	5.37	±0.17	3.57	±0.20
^{3}He	12.2	1.31	±0.04	0.46	±0.03	2.85	±0.22
^{3}He	24.4	0.21	±0.02	(a)		(a)	

(a) Count rate at 30 degrees was equal to the background of 0.46 ± 0.02 within the statistical uncertainties.

The field of view of the detector in all our experiments was larger than the source, so the thermal neutron count rate (0 degrees) was expected to decrease approximately as $1/r^2$ times the attenuation in air. This was approximately true as shown by the data in Table 4.1

Note that count rate at 30 degrees also falls off with distance from the source. This indicates that much of the 30-degree count rate is due to the source—most likely from epithermal neutrons that penetrate the Cd shield and are captured directly without thermalization.

4.1.6 Interference from Secondary Moderators

An important question in using narrow-field-of-view detectors is whether the presence of massive amounts of moderator away from the source could interfere with locating the source. To check this possibility, we placed the ^{3}He neutron detector 3.05 m from a 5.08-cm thick by 30.5-cm square block of polyethylene. The 30.5-cm-square face of the polyethylene was oriented at 45 degrees to the detector. The bare PuBe neutron source was located 3.05 m from the polyethylene on a line perpendicular to the line from the detector to the source. This arrangement should allow neutrons thermalized and scattered from the face of the polyethylene to reach the neutron detector (reflection geometry). The neutron count rate was measured as a function of orientation angle of the detector. As shown above, we did not expect to see any effect of the bare neutron source on the detector count rate as the detector orientation was varied. The count rate data are plotted in Figure 4.8. No statistically significant effects were seen at the angles corresponding to either the neutron source or the moderator block.

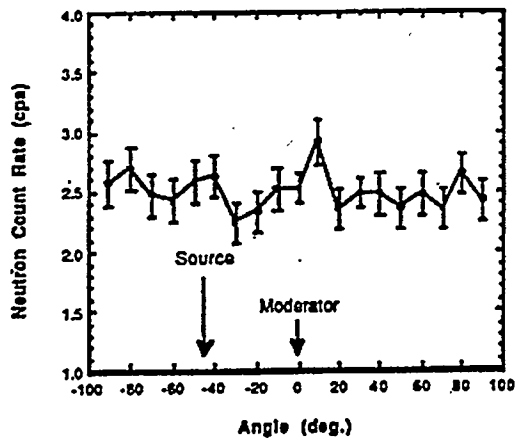

Figure 4.8. Neutron Count Rate as a Function of Detector Orientation Angle When Viewing a Neutron Source at -45 Degrees and a Moderator Block at 0 Degrees. A constant background of 0.32 ± 0.01 cps has been subtracted.

This null effect is produced because the polyethylene moderator sees only a small fraction of the solid angle of the neutron source, and the neutron detector sees only a small fraction of the solid angle of the polyethylene. In an effort to maximize any possible effect, the neutron source was moved to a position 0.91 m from the polyethylene. This position was just outside the field of view of the neutron detector. Data were obtained with the detector oriented at the neutron source (-17 degrees), at the moderator (0 degrees), and beyond the field-of-view of the moderator (+17 degrees). Count rates were measured using the reflection geometry described above and a transmission geometry in which the neutrons had to pass through the 5.08-cm-thick moderator before escaping towards the detector. As shown in Table 4.2, a small increase in count rate is a possibility when viewing the moderator under these conditions.

Table 4.2. Neutron Count Rates for Moderator Interference Tests. A background of 0.32 ± 0.01 cps has been subtracted.

Angle (degrees)	View	Net Count Rate (cps)
Reflection Geometry		
-17	Source	3.06 ± 0.06
0.00	Moderator	3.17 ± 0.06
+17	BGD	3.00 ± 0.06
Transmission Geometry		
-17	Source	3.11 ± 0.06
0.00	Moderator	3.18 ± 0.06
+17	BGD	3.08 ± 0.06

4.2 Gandolphi Diffractometry

Every crystalline material produces a unique diffraction pattern when struck with a *parallel* beam of x-rays. The individual features in the pattern can be used to discern the orientation and separation of the various crystal planes within the material. A related technique, powder diffractometry, uses a high-intensity beam of monoenergetic x-rays to analyze or simply identify a powdered crystalline material. For applications involving small or poor powder samples, many hours may be required to acquire a diffraction image as a result of limitations in the intensity of available x-ray beams.

Capillary x-ray lenses may ultimately make possible significant improvements in powder diffractometry technology. Figure 4.9 diagrams the methods used to acquire a powder diffraction pattern both with and without a capillary lens. The lens used will generally be of the "full barrel" type since it is desirable to maximize the transfer of radiation from the point-like source to the powder sample. Although the source-to-powder distance is significantly greater when the lens is used, the intensity gain of the lens is large enough to guarantee that more x-rays strike the powder sample.

This type of application is typical of those applications for which the divergence of the incident radiation beam is of primary importance. The divergence of the incident beam is critical since it determines the degree of "spreading" in the diffraction pattern. X-rays that reach the sample from different directions (which is possible only with the lens) produce diffraction patterns that travel in correspondingly different directions. A capillary lens clearly delivers more radiation to the sample, but the acquired image may be of inferior quality.

We have undertaken a series of experimental measurements in an attempt to verify the potential benefit to powder diffractometry arising from a capillary x-ray lens. A lens was purchased for use with an existing, state-of-the-art powder diffractometer. The main conclusions of this investigation are summarized below:

- The higher divergence (convergence) of the x-ray radiation that has passed through the lens greatly increases the difficulty of maintaining an acceptable control over background. The "beamstop" must in the future be carefully redesigned with this problem in mind.
- The relatively large focal lengths that are required for modern capillary lenses work against them in this case. The sample must be located 2 to 3 times farther with the lens than without. In the future, it may be possible to construct more compact lenses. This would be advantageous for this application.
- Any future improvements in either the efficiency or gain of capillary x-ray lenses would be helpful for this application. Such improvements are likely with the advent of monolithic lenses (see Section 5.0).
- It is critical that the x-ray source and x-ray lens be designed to work with each other. This specifically requires that the "spot size" of the x-ray generator must be minimized, something that is not of such paramount importance for many other applications. The x-ray lens in our experiments was unable to fully gather the x-ray radiation because of the small critical angle for acceptance and the finite "spot size."
- Our experiments demonstrated that the aperture used with the x-ray lens is of central importance to the quality and timeliness of the collected data. A large circular aperture results in a significant amount of x-ray radiation reaching the powder sample, but the result is relatively poor resolution and high background for the reasons already mentioned. A slit-like aperture is, for the special case of Gandolphi diffractometry, able to produce clear data in a way that is at least competitive with the no-lens arrangement. Optimization of the slit size and shape remains an important open question.
- The ultimate conclusion is that an x-ray lens appears to hold considerable promise for this application, but a re-design of the entire experimental setup would be required to realize these benefits.

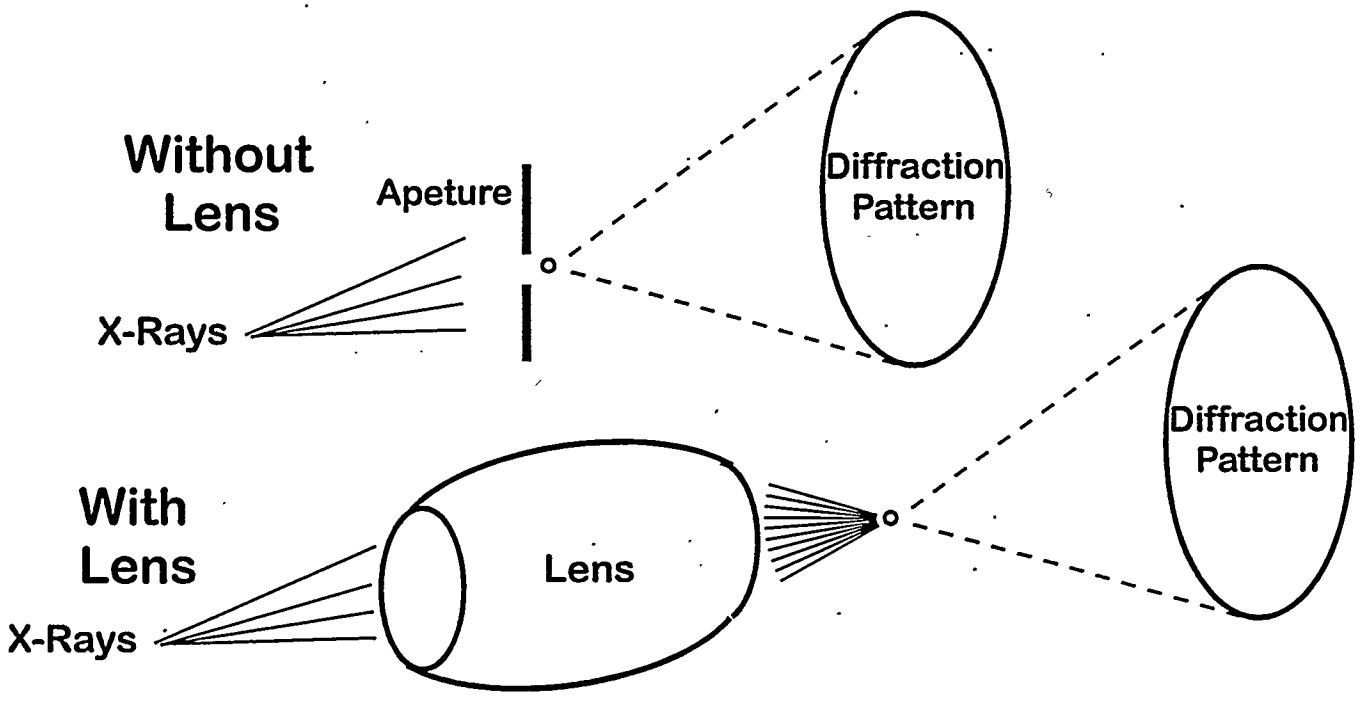

Figure 4.9. Acquiring a Powder Diffraction Pattern with and Without a Capillary X-ray Lens

4.3 Neutron Radiotherapy

Neutron capture therapy (NCT) takes place when thermal neutrons react with a reagent previously administered to a patient. The three primary characteristics of a successful reagent are 1) high thermal neutron cross section, 2) ease of incorporation in a pharmaceutical compound that is selectively absorbed by tumor cells, and 3) post-reaction delivery of high linear energy transfer radiation (energetic, short-range radiation). Currently, boron and gadolinium are favored reagents.

Currently, successful treatment of near-surface tumors has been demonstrated using thermal neutron beams (Hatanaka and Nakagawa 1994). Because of the limited ability of thermal neutrons to penetrate deeply in the hydrogenous material of the human body, however, such treatments are of little use for deep-seated tumors. One strategy for the treatment of such tumors requires the use of epithermal neutron beams (0.1eV to 10keV) with increased penetration (Barth et al. 1990; Slatkin 1991; Harling 1994). However, the generation of sufficiently strong and pure epithermal beams is difficult. In addition, the use of epithermal neutrons inevitably leads to the irradiation of an excessively large region within the patient.

Capillary neutron optics makes possible a novel approach to delivering neutrons to a patient (Peurrung 1996). Figure 4.10 shows a system that uses a neutron lens to allow delivery of thermal neutrons directly to a medically optimal location deep within the patient. The major components of this treatment system are the moderator, lens, treatment tube, and shield. The sole function of the moderator is to provide a source of cold neutrons that can be focused by the lens. This moderator is typically small (roughly 1 cm in diameter), and must be maintained at a relatively low temperature (20K) to optimize the performance of the lens. The treatment tube in turn provides an open space free of hydrogenous material through which neutrons are able to travel unimpeded.

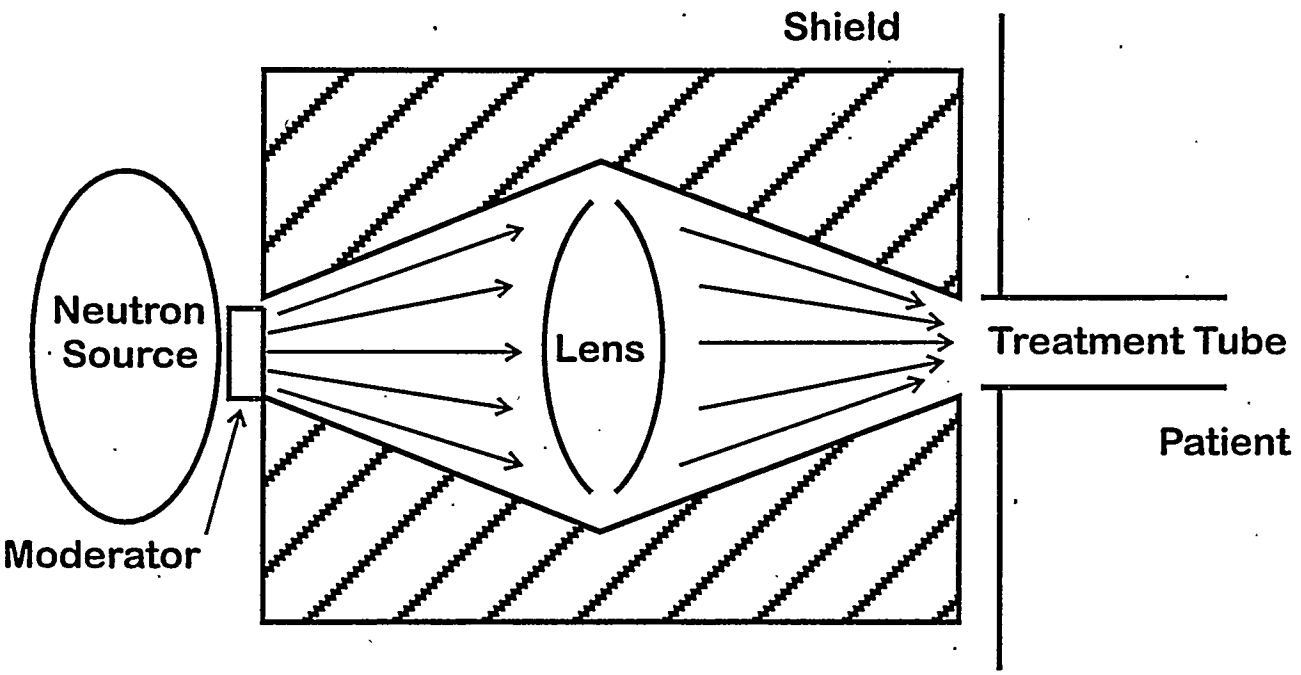

Figure 4.10. Side-View Schematic of a Capillary Lens-based Neutron Radiotherapy Treatment Beamline

This treatment system has several important advantages. It uses a relatively straightforward subthermal neutron source, yet allows the treatment of deep tumors normally accessible with only epithermal beams. In addition, the limited penetration of thermal neutrons spares the patient from unnecessary irradiation of healthy tissue. Finally, nearly complete shielding of the patient from unwanted source radiation is possible with this simple and compact beamline. Shielding may ultimately be placed within the lens in the empty spaces between the polycapillaries.

A unique characteristic of this application is that importance is placed on maximizing the total neutron fluence (measured in neutrons/second) delivered to the tumor. Most lens applications instead measure performance in terms of flux intensity gain. (Neutron flux is measured in neutrons/[second•cm^2].) The lens makes it possible to deliver a large neutron fluence in the form of a beam that is sufficiently compact and collimated to travel the length of the treatment tube. This application tends to favor large-area lenses that have superior neutron gathering power and lenses with long focal lengths to achieve the minimum treatment tube width.

The results described in this subsection were achieved under a project funded by laboratory directed research and development funds. PNNL has applied for a patent on this technology.

5.0 Discussion and Conclusion

Capillary lenses are likely to have a significant impact in a number of different areas where x-rays or low energy neutrons are important. When considering the application of these lenses to specific problems, it is essential to carefully consider their advantages, disadvantages, capabilities, and limitations. The following is a brief, itemized summary of many of the important principles.

- Lenses can be used for bending, focusing, collimation, or any combination thereof.
- Lens performance is highly energy-dependent: In general, only thermal (or colder) neutrons and 1 to 10 keV x-rays can be usefully focused.
- The capillaries in current lenses are limited to a radius of curvature of roughly 1 meter.
- Lenses currently tend to be no more than several centimeters in diameter and several tens of centimeters in length. Lenses with dimensions exceeding these limits may be expensive or perhaps less useful.
- Current lenses are roughly 20% efficient at focusing incident radiation that strikes at an angle less than the critical angle.
- Lenses cannot focus any radiation that strikes at an angle greater than the critical angle.
- The critical angle is typically between 1 and 5 milliradians.
- Focusing lenses can achieve intensity gains of roughly a factor of 100 because all of the transmitted radiation is brought to a focus that has a FWHM of roughly 0.5 mm or less.
- Radiation at the output focus of a capillary lens has been spatially "compressed" at the expense of increased divergence. Thus, any application for which collimated radiation is desirable may benefit less than expected when implemented with the aid of a capillary lens.

A natural question is whether capillary neutron lenses can be used to aid in monitoring thermal neutron emission from a distant neutron source. If the neutron radiation emanating from a distant moderated source could be brought to a narrow focus, a small, low-background neutron counter could be used for measurement. In this way, in principle, it might be possible to monitor neutron-emitting sources from distances much greater than are possible with conventional techniques. However, as is detailed in Section 4.1, such a neutron "telescope" suffers from a number of problems:

- Only a small component of the neutron radiation from a distant source is completely thermalized.
- The critical angle for thermal neutron radiation is only roughly 0.001 radians. Most neutron focusing applications use sub-thermal neutron radiation.
- Some of the thermal neutron radiation scatters between the source and the telescope. Because of the narrow acceptance angle of the lens, this radiation is sure to be missed by the detector.
- The small critical angle implies that the lens can accept only those neutrons that have been emitted from within 0.001 radians of the point that the telescope is "aimed" at. At a distance of 50 meters, this size is only 10 centimeters in diameter. Thus, the telescope would only work well for relatively compact sources.

- The relatively small size of the lens itself limits the neutron gathering power of a monitoring system implemented in this way.

Despite these limitations; a neutron telescope appears to be possible with current technology. More importantly, future improvements in lens capability will improve the likelihood that a neutron telescope will provide a useful means for neutron monitoring from 50 meters or more. Possible future improvements may include the development of ^{58}Ni-coated lenses for increased neutron focusing power and the development of monolithic lenses with a greatly reduced focal spot size.

6.0 References

Barth RF, AH Soloway, and RG Fairchild. 1990. "Boron Neutron Capture Therapy for Cancer," *Sci. Amer.*, **263**, p. 100.

Chapman HN, KA Nugent, and SW Wilkins. 1993. "X-ray focusing using cylindrical-channel capillary arrays," *Appl. Opt.*, **32**, p. 6333.

Chen H, RG Downing, DFR Mildner, WM Gibson, MA Kumakov, IYu Ponamarev, and MV Gubarev. 1992. Guiding and Focusing Neutron Beams Using Capillary Optics," *Nature* **357**, p. 391.

East LV and RB Walton. 1969. "Polyethylene moderated ^{3}He neutron detectors," *Nucl. Instrum. Meth.*, **72**, p. 161.

Fraser GW, AN Brunton, JE Lees, and DL Emberson. 1993. "Production of quasi-parallel x-ray beams using microchannel plate x-ray lenses," *Nucl. Inst. Meth. in Phys. Res. A*, **334**, p. 579.

Harling OK. 1994. "Boron Neutron Capture Therapy at the MIT Research Reactor," *Neut. News* **5**, p. 23.

Hatanaka H and Y Nakagawa. 1994. "Clinical Results of Long-Surviving Brain Tumor Patients who Underwent Boron Neutron Capture Therapy," *Int. J. Radia. Onc., Biol., and Phys.*, **28**, p. 1061.

Hoffman SA, DJ Thiel, and DH Bilderback. 1994. "Applications of Single Tapered Glass Capillaries: Submicrometer X-Ray Imaging and Laue Diffraction," *Opt. Eng.*, **33**, p.303.

Kaaret P, P Geissbuhler, A Chen, and E Glavinas. 1992. "X-ray focusing using microchannel plates," *Appl. Opt.*, **31**, p. 7339.

Kimball JC and D Bittel. 1993. "Surface Roughness and the Scattering of Glancing-Angle X-Rays: Application to X-Ray Lenses," *J. Appl. Phy.*, **74**, p. 877.

Kumakov MA and FF Komarov. 1990. "Multiple Reflection from Surface X-ray Optics," *Phys. Rpts*, **191**, p.289.

Ullrich JB, V Kovantsev, and CA MacDonald. 1993. "Measurements of polycapillary X-ray optics." *J. Appl. Phys.*, **74**, (no.10):5933-9.

Marten L. 1966. "X-Ray Fiber Optics," *Appl. Phys. Lett.*, **9**, p. 194.

Mildner DFR. 1990a. "Neutron Focussing Using Microguides," *Nucl. Inst. Meth. in Phys. Res. A*, **297**, p. 38.

Mildner DFR. 1990b. "Multiple Reflections within Neutron Optical Devices," *Nucl. Inst. Meth. in Phys. Res. A*, **292**, p. 693.

Mildner D, H Chen, G Downing, and V Sharov. 1993. "Focused Neutrons: A Point to be Made," *J. Neut. Res.*, **1**, p. 1.

Mildner DFR, H Chen-Mayer, and VA Sharov. 1995. "Restricted Neutron Transmission Through a Cylindrical Guide Tube," *J. Appl. Cryst.*, **28**, pt. 6:793-802.

Mosher D and SJ Stephanakis. 1976. "X-ray 'Light pipes,'" *Appl. Phys. Lett.*, **29**, p.105.

Pantell RH and PS Chung. 1979. "Influence of Surface Roughness on the Propagation of X-Rays through Capillaries," *Appl. Opt.*, **18**, p. 897.

Pantojas VM, VE Kovantsev, J Pant, SA Budkov, TM Hayes, and PD Persans. 1993. "A Polycapillary-Based X-Ray Optical System for Diffraction Applications," *Nucl. Inst. Meth. in Phys. Res. A*, **333**, p. 607.

Peurrung AJ. 1996. "Capillary Neutron Optics for Radiotherapy," *Med. Phys.*, **23**, p. 487.

Slatkin DN. 1991. "A History of Boron Neutron Capture Therapy of Brain Tumors," *Brain*, **114**, p. 1609.

Stoffels JJ and DR Ells. 1979. *Rev. Sci. Instr.* **50**, p. 1574.

Thiel DJ, EA Stern, DH Bilderback, and A Lewis. 1989. "Focusing of Synchrotron Radiation using Tapered Glass Capillaries," *Physica B*, **158**, p. 314.

Vanier PE, L Forman, and EC Selcow. 1995. "A thermal neutron source imager using coded apertures." *In: Proceedings of the Institute of Nuclear Materials Management*, Palm Desert, California, July 9-12, 1995, p. 842.

Xiao QF, IYu Ponamarev, AI Kolomitsev, and JC Kimball. 1993. "Numerical simulations for capillary-based x-ray optics," in "Multilayer and grazing incidence x-ray/EUV Optics II." *Proceedings of the International Society for Optical Engineering*, RB Hoover and A Walker, editors, San Diego, California, Vol. 1736, pp. 227-238.

Distribution

No. of Copies

Offsite

2 DOE Office of Scientific and Technical Information

Harold Beck
DOE/EML
201 Varick Street
5th Floor
New York, New York 10014-4811

A.J. (Gus) Caffrey
Idaho National Engineering Laboratory
P.O. Box 1625
Idaho Falls, Idaho 83415

Charles Dickerman
Argonne National Laboratory
9700 South Cass Avenue
RE/208
Argonne, Illinois 60439-4842

Tom Gosnell
Lawrence Livermore National Laboratory
P.O. Box 808
Livermore, California 94550

David Gordon
Brookhaven National Laboratory
Department of Advanced Technologies
Building 197C
P.O. Box 5000
Upton, New York 11973-5000

M. William (Bill) Johnson
Los Alamos National Laboratory
P.O. Box 1663
Los Alamos, New Mexico 87545

No. of Copies

John Mihalczo
Oak Ridge National Laboratory
Building 3500
P.O. Box 2008
Oak Ridge, Tennessee 37831-6004

Dick Pollina
Bechtel Nevada/NTS
P.O. Box 98521
Las Vegas, Nevada 89193-8521

David Spears
Forrestal Building
U.S. Department of Energy
1000 Independence Avenue, SW
Washington, DC 20585

Dave Waymire
Sandia National Laboratory
Systems Research Center 5900
P.O. Box 5800
Albuquerque, New Mexico 87185

Willard Winn
Westinghouse Savannah River
Technology Center (SRTC)
P.O. Box 130
New Ellenton, South Carolina 29809

Onsite

32 *Pacific Northwest National Laboratory*

M Bliss
RA Craig
GB Dudder
EA Lepel
AJ Peurrung (10)
PL Reeder (5)
DE Robertson
DC Stromswold
DS Sunberg(2)
J Wacker
RA Warner(3)
Technical Report Files (5)